Journal of Medicinal Chemistry

Article

Towards a Rational Design of Polyamine-based Zinc Chelating Agents for Cancer Therapies

Cristina Galiana-Roselló, Clara Aceves-Luquero, Jorge González, Álvaro Martínez-Camarena, Ruth Villalonga, Silvia Fernández de Mattos, Concepción Soriano, José Llinares, Enrique García-España, Priam Villalonga, and María Eugenia González-Rosende

J. Med. Chem., **Just Accepted Manuscript** • DOI: 10.1021/acs.jmedchem.9b01554 • Publication Date (Web): 14 Jan 2020

Towards a Rational Design of Polyamine-based Zinc Chelating Agents for Cancer Therapies

Cristina Galiana-Roselló,[†,∇,*] Clara Aceves-Luquero,[‡] Jorge González,[†] Álvaro Martínez-Camarena,[†] Ruth Villalonga,[⊥] Silvia Fernández de Mattos,[‡,§] Concepción Soriano,[‖] José Llinares,[‖] Enrique García-España,[†,*] Priam Villalonga,[‡,*] María Eugenia González-Rosende[∇,*]

[†]*Instituto de Ciencia Molecular (ICMol), Departamento de Química Inorgánica, Universidad de Valencia, 46980-Paterna, Valencia, Spain.*

[‡]*Cancer Cell Biology Laboratory, Institut Universitari d'Investigació en Ciències de la Salut (IUNICS), Universitat de les Illes Balears, and Institut d'Investigació Sanitària Illes Balears (IdISBa), 07122-Palma, Illes Balears, Spain.*

[§]*Departament de Biologia Fonamental, Universitat de les Illes Balears, 07122-Palma, Illes Balears, Spain.*

[⊥]*Departament de Química, Universitat de les llles Balears, 07122-Palma, Illes Balears, Spain.*

[‖]*Departamento de Química Orgánica, Universidad de Valencia, C/Dr. Moliner s/n, 46100-Burjassot, Valencia, Spain.*

[∇]*Departamento de Farmacia, Facultad de Ciencias de la Salud, Universidad CEU Cardenal Herrera, C/ Ramón y Cajal, s/n, 46115-Alfara del Patriarca, Valencia, Spain.*

ABSTRACT: *In vitro* viability assays against a representative panel of human cancer cell lines revealed that polyamines **L1a** and **L5a** displayed remarkable activity with IC_{50} values in the micromolar range. Preliminary research indicated that both compounds promoted G1 cell cycle arrest followed by cellular senescence and apoptosis. The induction of apoptotic cell death involved loss of mitochondrial outer membrane permeability and activation of caspases 3/7. Interestingly, **L1a** and **L5a** failed to activate cellular DNA damage response. High intracellular zinc chelating capacity of both compounds, deduced from the metal specific *Zinquin* assay and Zn**L**$^{2+}$ stability constant values in solution strongly support their cytotoxicity. These data along with quantum mechanical studies have enabled to establish a precise Structure-Activity Relationship. Moreover, **L1a** and **L5a** showed appropriate drug-likeness by *in silico* methods. Based on these promising results, **L1a** and **L5a** should be considered a new class of zinc-chelating anticancer agents that deserve further development.

INTRODUCTION

Cancer is a major public health problem and represents the second leading cause of death worldwide.[1] According to WHO estimates, it accounted for over 9.6 million deaths in 2018. Moreover, the number of new cases is expected to rise by about 70% over the next two decades with over 20 million new cancer cases annually (particularly in low- and middle-income countries).[2] These considerations have led to increased research in order to provide effective anticancer therapies. Clinical treatments include various therapeutic modalities such as surgery, radiotherapy, and chemotherapy. Despite overwhelming advances in cancer research and clinical oncology, the need to provide more effective treatments encourages the search for New Molecular Entities (NMEs) including small molecule- and biologic–based drugs.[3] Many chemotherapeutic agents have been developed and the number of NMEs targeting cancer has grown impressively since the 1990s; unfortunately, the clinical use is still associated with severe adverse reactions and the rapid development of resistance. Therefore, the search for highly effective and safer anticancer drugs is an essential and urgent need and continues to be a formidable challenge.

The enormous structural diversity of Natural Products (NPs) and their medicinal significance have led researchers to establish NPs as lead compounds. As a result, a significant number of natural product-based drugs have been introduced into the market over the years. At present, more than 100 new products are in clinical development, particularly as anticancer and anti-infective agents.[4] Recently, a great deal of attention has been focused on the naturally occurring and biologically active polyamines, e.g. Spermidine (Spd), Spermine (Spm) and their 1,4-diaminobutane precursor Putrescine (Put). These natural polyamines are involved in a large number of fundamental biological processes and play an important role in eukaryotic cell proliferation, differentiation, and death. Moreover, polyamine homeostasis has long been known to be dysregulated in various pathological conditions, most notably in cancer. High levels of polyamines have been observed in breast, colon, prostate and skin cancers. In addition, anomalous levels of biosynthetic and catabolic rate-limiting enzymes of polyamine metabolism have been

detected. [5] Consequently, polyamines represent a universal template due to their many physiological and/or pathological roles.[6] It is well-known that polyamine analogues exhibit considerable potential as cytotoxic agents for cancer chemotherapy. Recent studies have focused on the discovery of compounds that produce cellular effects that are either independent, or in addition to the polyamine metabolic enzymes.[5b,7]

Another group of compounds extensively used in cancer research are metal-sequestering agents.[8] Metals including iron, copper and zinc are essential for physiological processes.[8c,9] Remarkably, Zn^{2+} plays a vital role in numerous cellular processes such as survival, proliferation, and apoptosis, both in normal and in cancer cells.[10] Moreover, many reports have shown that both increase and decrease in Zn^{2+} levels are associated with cancer development. Thus, depletion of cellular zinc by chelating agents has been proposed as a strategy for treatment of cancers.[10-11] On the other hand, polyamines are suitable ligands for metal ions such as Pd^{2+}, Pt^{2+}, $Fe^{(2+/3+)}$, $Cu^{(1+/2+)}$ or Zn^{2+}. Numerous studies have reported that polyamines yield polynuclear chelates with antiproliferative activities.[9b,9d,12] Recently, it has been demonstrated that the polyamine *N,N,N´N´*-tetrakis(2-pyridilmethyl)ethylenediamine (TPEN), a membrane–permeable zinc chelator, shows pro-apoptotic effects on human acute promyelocytic leukemic cells in addition to solid tumor cells, indicating that Zn^{2+} depletion can be a potential strategy for cancer treatment.[13]

Given the aforementioned findings, in our search for new anticancer agents,[14] we synthesized a small library of polyamine derivatives through a pharmacomodulation design strategy based on the natural polyamine Spermidine and performed a first evaluation of their biological activity. Our design concept was based on modifying the chain length of the Spd core framework with the substitution of the three/four methylene chains of spermidine backbone by ethylene groups and the insertion of appropriate substituents on the terminal and central amino groups (Figure 1). In this paper, we report the synthesis of a series of polyamine analogues considering our design strategy, and the evaluation of their potential anticancer activity against a broad panel of human cancer cells. The cellular effects on cell cycle progression, senescence, apoptosis and DNA damage-inducing capability of the most active compounds are analyzed. In addition, intracellular zinc chelating ability of selected polyamines as a potential mechanism of action and, their zinc binding affinity and coordination mode are investigated. Finally, the Structure Activity Relationship (SAR) is explored to define which features are necessary for the anticancer activity, and the drug-likeness properties of the most active compounds is evaluated in order to design new lead anticancer drug candidates for future synthesis and biological testing.

RESULTS AND DISCUSSION

Chemistry. With the goal to develop an inexpensive and straightforward synthetic strategy to prepare our library of polyamine compounds, we based the synthesis on the commercially available 1,4,7-triazaheptane (DIEN). In order to introduce structural diversity in the library, we combined two structural domains D1 and D2 on DIEN scaffold. Thus, we explored both the functionalization of central (D1) and terminal amino groups (D2) by insertion of the building blocks R_1 and R_2. According to the functionalization of the central nitrogen (R_1), we classified the compounds in

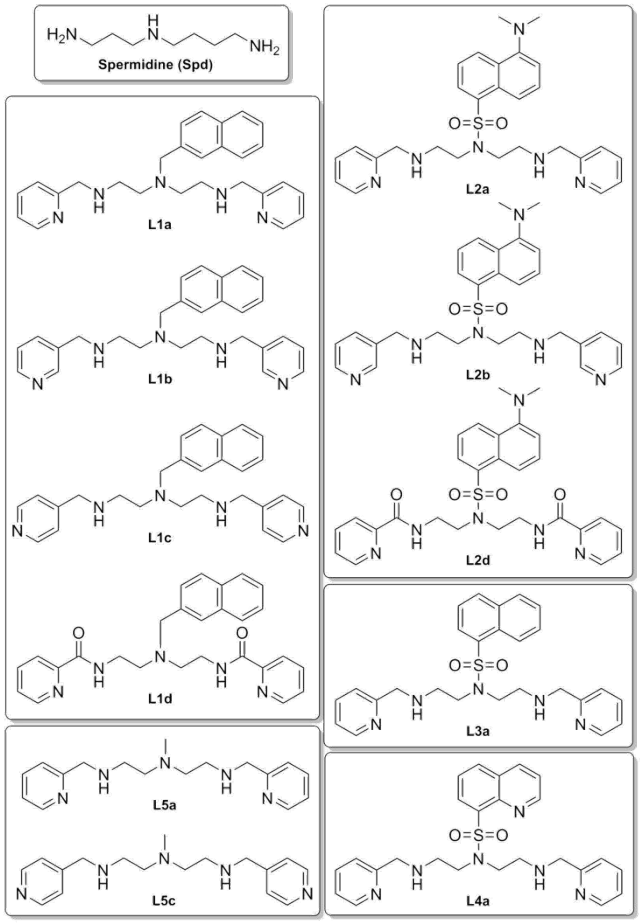

Figure 1. Library of synthesized polyamine compounds.

five series **L1**-**L5**, and depending on the functionalization of the terminal amino groups (R_2) as **a**-**d** (Figure 2).

Considering the design pattern, we obtained eleven polyamine derivatives in high yields (Figure 1). The target compounds were synthesized as outlined in Scheme 1 and Scheme 2 following a four-step route starting from the commercial DIEN (**L**), according to previously reported procedures[15]: 1) Protection of **L** terminal amino groups with an excess of phthalic anhydride (2.2 equiv) to afford the protected amine **L-ft**; 2) **L-ft** central nitrogen alkylation or sulfonylation by nucleophilic attack of the corresponding alkyl or arylsulfonyl halides to give 3-*N*-substituted diphthalimides **L-(1-4)-ft**, and 3) removal of the protecting groups with hydrazine in ethanol to give the free alkylated polyamines **L1**-**L4** (Scheme 1).

The last step is shown in Scheme 2. Compounds **L1**-**L4** as well as the commercial polyamine 4-methyl-1,4,7-triazaheptane **L5** were reacted with pyridinecarboxaldehydes **a-c** (1:2 ratio), and the corresponding imines were subsequently reduced *in situ* with $NaBH_4$ to afford compounds **L1a-c**, **L2a,b**, **L3a**, **L4a** and **L5a,c**. In addition, we synthesized two carboxamide derivatives **L1d** and **L2d** by reacting polyamines **L1** and **L2** with methyl picolinate **d**, as illustrated in Scheme 2. All the compounds were fully characterized by 1D (^1H, ^{13}C, DEPT)

and 2D (COSY, HSQC) NMR spectroscopy, HR-MS and elemental analysis. The spectra of compounds not previously described are provided in the

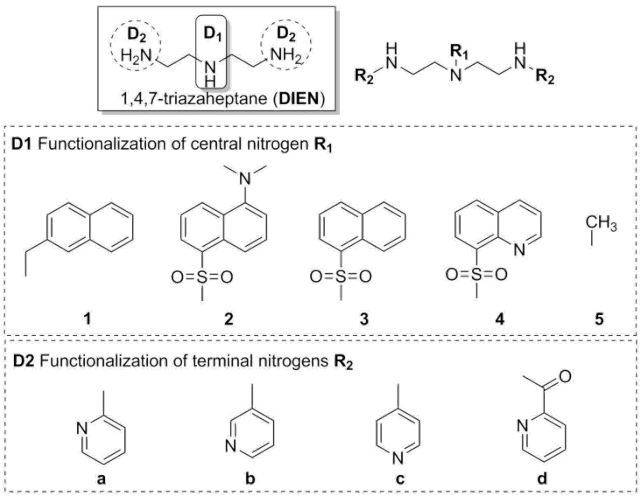

Figure 2. Design strategy and structural diversity domains D1 and D2 on polyamine skeleton.

Scheme 1. Synthesis of amines L1-L4.[a]

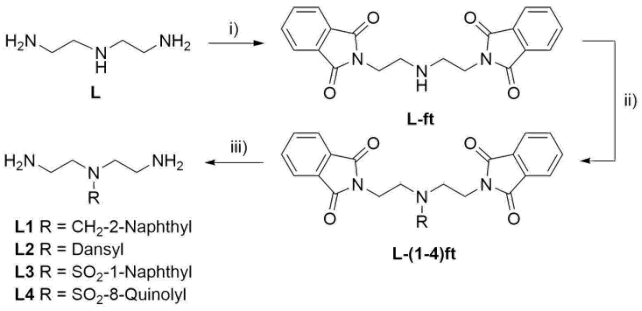

[a]Reagents and conditions: i) Phthalic anhydride (2.2 equiv), CH_3COOH, reflux, 1.5 h; ii) 2-NaphthylCH_2Br or R_1SO_2Cl (R_1 = Dansyl, Naphthyl, 8-Quinolyl), K_2CO_3 (1.6 equiv), CH_3CN, reflux, 24 h; iii) N_2H_4, EtOH, reflux, 24 h.

Electronic Supplementary Information (ESI, Figures S1.1-S1.42).

Biological activities. **Antiproliferative activities**. The inhibitory activity of polyamine derivatives **L1-L5** was first investigated *in vitro* using a panel of representative human cancer cell lines, including cells from both hematological malignancies, such as leukemia (Jurkat) and lymphoma (Jeko-1) and solid tumors (LN229, U87MG). Cell viability was evaluated after 48 h upon 10 μM treatment with polyamines **L1-L5** by using a luminescent-based ATP assay. The results showed that out of the eleven tested polyamines, two compounds **L1a** and **L5a** displayed a significant antiproliferative activity across the panel (ESI, Figure S3).

Based on the positive results obtained with compounds **L1a** and **L5a**, we tested them against additional cell lines, including Granta-519, Z-138, JMV-2, UPN-2, SP53, SKMG-3, PC3, MCF-7, SW480 and SW620 human cancer cell lines. The analysis of the antiproliferative activity indicated that both compounds had high cytotoxic profiles. Interestingly compound **L5a** exhibited higher efficacy than compound **L1a** (Figure 3A). In agreement with their effects on cell viability, phase-contrast microscopy indicated that treatment with **L1a** and **L5a** reduced LN229 and PC-3 cell proliferation and provoked morphological changes consistent with the induction of cell death. Thus, cells treated with **L1a** or **L5a** exhibited several apoptosis-specific features such as loss of cellular adherence, cell rounding and shrinkage, followed by moderate and rather random membrane blebbing,

Scheme 2. Functionalization of terminal amino groups of polyamines L1-L5.[a]

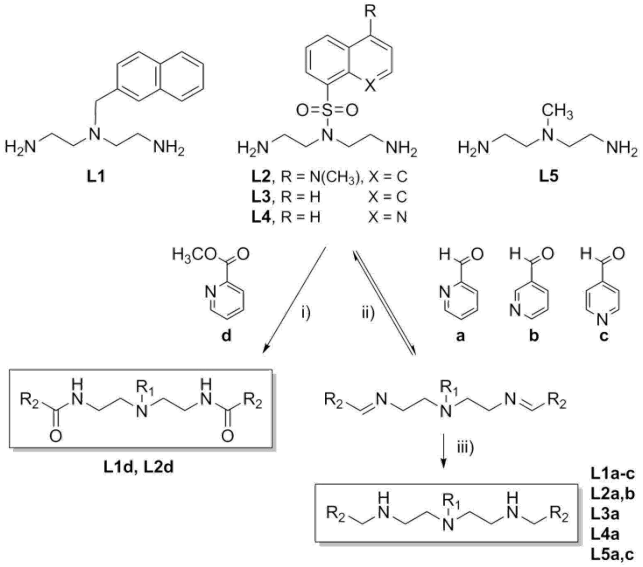

[a]Reagents and conditions: i) MeOH, reflux, 48 h; ii) EtOH, rt, 4 h; iii) $NaBH_4$ (6 equiv), EtOH, rt, 24 h.

in comparison with the compact rounded nucleus of vehicle-treated cells (Figure 3B). In addition, dose-response experiments indicated that compounds **L1a** and **L5a** were capable of inducing a pharmacologically relevant antiproliferative activity in the low micromolar range with IC_{50} values ranging from 1.99 μM (Jurkat) to 11 μM (PC3) after a 48 h drug exposure. Moreover, we have also tested the cytotoxic effects of polyamines **L1a** and **L5a** on fibroblast cells from individuals. A significantly higher sensitivity of the cancerous cells as compared to non-cancerous cells was observed, highlighting the potential selectivity of **L1a** and **L5a** (Figure 3C).

Cell Cycle Perturbations and Senescence Induction. Many anticancer drugs promote cancer cell growth arrest or cell death. To gain insight into the mechanisms through which polyamines **L1a** and **L5a** reduce cell viability, we next proceeded to characterize their cellular effects.

In order to analyze the impact of polyamines **L1a** and **L5a** on cell cycle progression, flow cytometric analysis upon propidium iodide staining after 24 and 48 h treatment periods was performed in LN229, U87MG, PC-3 and Jurkat cells. The results showed that both compounds induced a remarkable increase in the G0/G1 population of the cell cycle

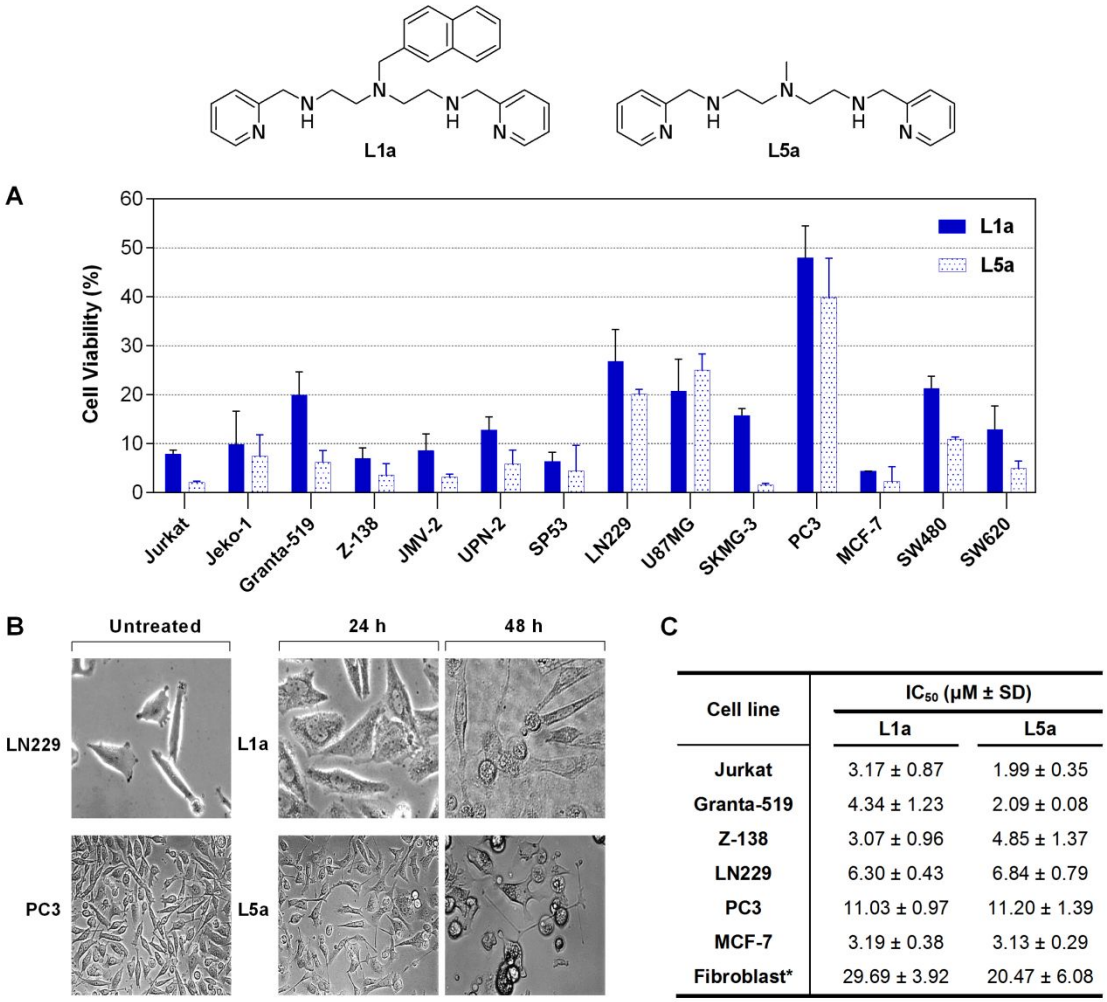

Cell line	IC_{50} (μM ± SD)	
	L1a	L5a
Jurkat	3.17 ± 0.87	1.99 ± 0.35
Granta-519	4.34 ± 1.23	2.09 ± 0.08
Z-138	3.07 ± 0.96	4.85 ± 1.37
LN229	6.30 ± 0.43	6.84 ± 0.79
PC3	11.03 ± 0.97	11.20 ± 1.39
MCF-7	3.19 ± 0.38	3.13 ± 0.29
Fibroblast*	29.69 ± 3.92	20.47 ± 6.08

Figure 3. Inhibitory effect on cell viability of L1a and L5a in a tumor cell line panel. (A) The indicated cell lines were treated for 48 h with 10 μM **L1a** and **L5a**. The mean ± SD values from three independent experiments each conducted in triplicate are shown in the graph, representing the percentage of viable cells relative to untreated conditions. (B) Representative phase-contrast photomicrographs of LN229 and PC3 cells after the indicated time-points exposure with 10 μM **L1a** and **L5a**. (C) IC_{50} mean values ± SD for the indicated cell lines, obtained from three independent experiments, each conducted in triplicate. *Fibroblast cells derived from individuals.

along with a slight compensatory decrease in the G2 phase in all the tested cell lines (Figure 4A). Moreover, we also observed hypodiploid sub-G1 cells consistent with induction of apoptosis after 48 h treatment in PC-3 cells (Figure 4B).

We next analyzed the induction of cellular senescence upon **L1a** and **L5a** treatment performing a standard senescence assay based on the quantification of *β*-galactosidase positivity[16] (Figures 4C-D). Whereas untreated LN229 and PC-3 cells were *β*-gal negative, treatment with **L1a** and **L5a** both led to a clear increase in the proportion of *β*-gal positive cells after 24 h treatment. Interestingly, despite the observation that both cell lines showed a similar IC_{50} value for both compounds (Figure 3C), the percentage of senescent cells was significantly higher upon treatment with **L1a**, since this compound promoted up to a 90% of senescence in LN229 cells and a 50% in PC-3 cells (Figure 4C). Phase-contrast photomicrographs of LN229 and PC-3 cells after 24 h treatment with 10 μM **L1a** and **L5a** showed characteristic morphological changes associated with the induction of cellular senescence such as flattened, wider and irregular cell shapes, larger volumes and increased nuclear size, especially in **L1a**-treated LN229 cells (Figure 4D).

Overall, these data indicate that the prolonged cell cycle arrest induced by compounds **L1a** and **L5a** also leads to the induction of the cellular senescence program.

Induction of Apoptosis. We next assessed whether polyamines **L1a** and **L5a** were able to promote cellular death. For this purpose, we investigated the ability of **L1a** and **L5a** to induce apoptosis by performing a combined approach including measurements of executioner caspases activation, Mitochondrial Membrane Potential (MMP, $\Delta\Psi_m$) and Annexin V-FITC/PI staining (Figure 5).

Caspases 3/7 are key proteases in apoptosis and are considered the main executioner caspases in which both the intrinsic and extrinsic apoptotic pathways converge. We thus monitored caspase 3/7 activity in a panel of human

cancer cell lines upon cell treatment with **L1a** and **L5a** (10 μM for 48 h) using the Caspase–Glo 3/7 luminescence assay. The

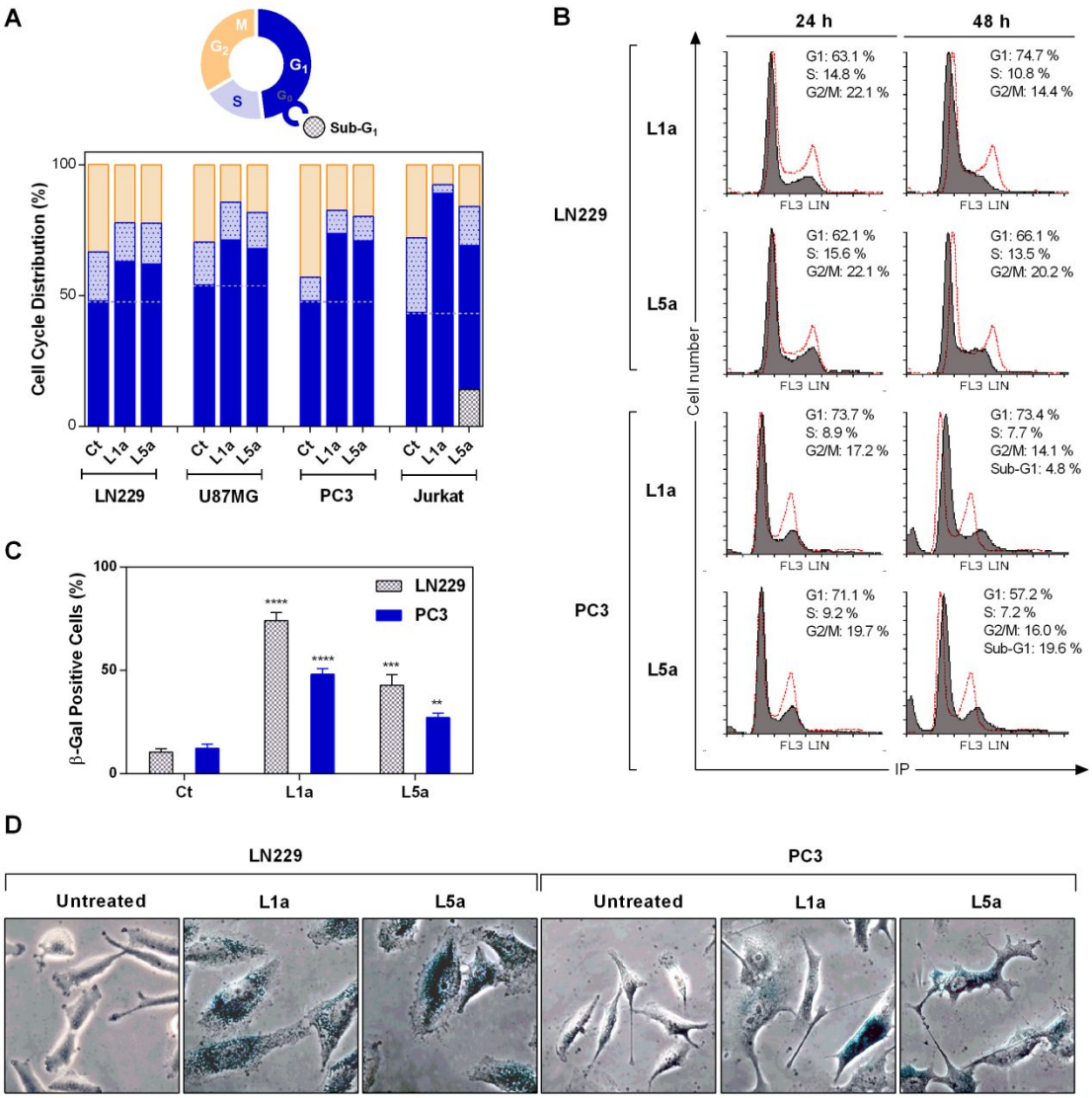

Figure 4. Polyamines **L1a** and **L5a** induce G1 cell cycle arrest and promote the accumulation of senescent cells. (**A**) and (**B**) Cell cycle analysis. The indicated cell lines were left untreated or were treated for 24 h and 48 h with 10 μM **L1a** and **L5a**. Cells were harvested and their DNA content analyzed by flow cytometry as described in the Experimental Section. (A) The graph summarizes the percentage of cells at each phase of the cell cycle in control and **L1a-L5a**-treated conditions (24 h). (B) Representative histograms from three independent experiments are shown for each experimental condition. (**C**) and (**D**) senescence associated β-galactosidase (SA-*β*-gal) staining. (C) Quantitation of positively stained cells. LN229 and PC-3 cells were left untreated or treated for 24 h with 10 μM **L1a** and **L5a** and stained for *β*-galactosidase as indicated in the Experimental Section. The graphs show the percentage of SA-*β*-gal-positive cells related to untreated conditions as measured from ten different fields from four independent experiments. Bars represent mean ± SD. Statistical significance was determined by Student's *t*-test (**p<0.01; ***p<0.001; ****p<0.0001). (D) Representative phase-contrast photomicrographs of LN229 and PC-3 cells after 24 h exposure with 10 μM **L1a** and **L5a** (original magnification ×100).

results revealed that treatment with both compounds induced a detectable increase in the activity of executioner caspases 3/7. Importantly, caspase activation inversely correlated with the reduction of cell viability induced by **L1a** and **L5a** treatment in most cell lines (Figure 5A). Mitochondrial membrane permeabilization constitutes an essential step of the intrinsic pathway leading to apoptosis, and the loss of MMP may be an early apoptotic event.[17]

Therefore, we investigated by flow cytometry the mitochondrial membrane potential of LN229 cells treated with polyamines **L1a** and **L5a** and stained with JC-1 dye. JC-1, a mitochondria selective aggregate dye, is a well-established marker to detect mitochondrial membrane

potential disruption during apoptosis.[18] The fluorescence variations of JC-1 in **L1a** and **L5a** treated cells implied that both compounds markedly altered the mitochondrial membrane potential (Figure 5B). The induction of apoptosis was finally confirmed using flow cytometry upon Annexin V/propidium iodide double staining. Annexin V is commonly used as an apoptosis marker due to its ability to detect phosphatidylserine externalization occurring on the membrane of apoptotic cells. Flow cytometry analysis indicated a significant shift of the PC-3 cellular population to the early and late apoptotic quadrant after 72 h treatment, reaching up to a 30 fold-increase in apoptosis in treated cells relative to untreated cells (Figures 5C, 5D). Altogether, these results collectively suggest that the broad

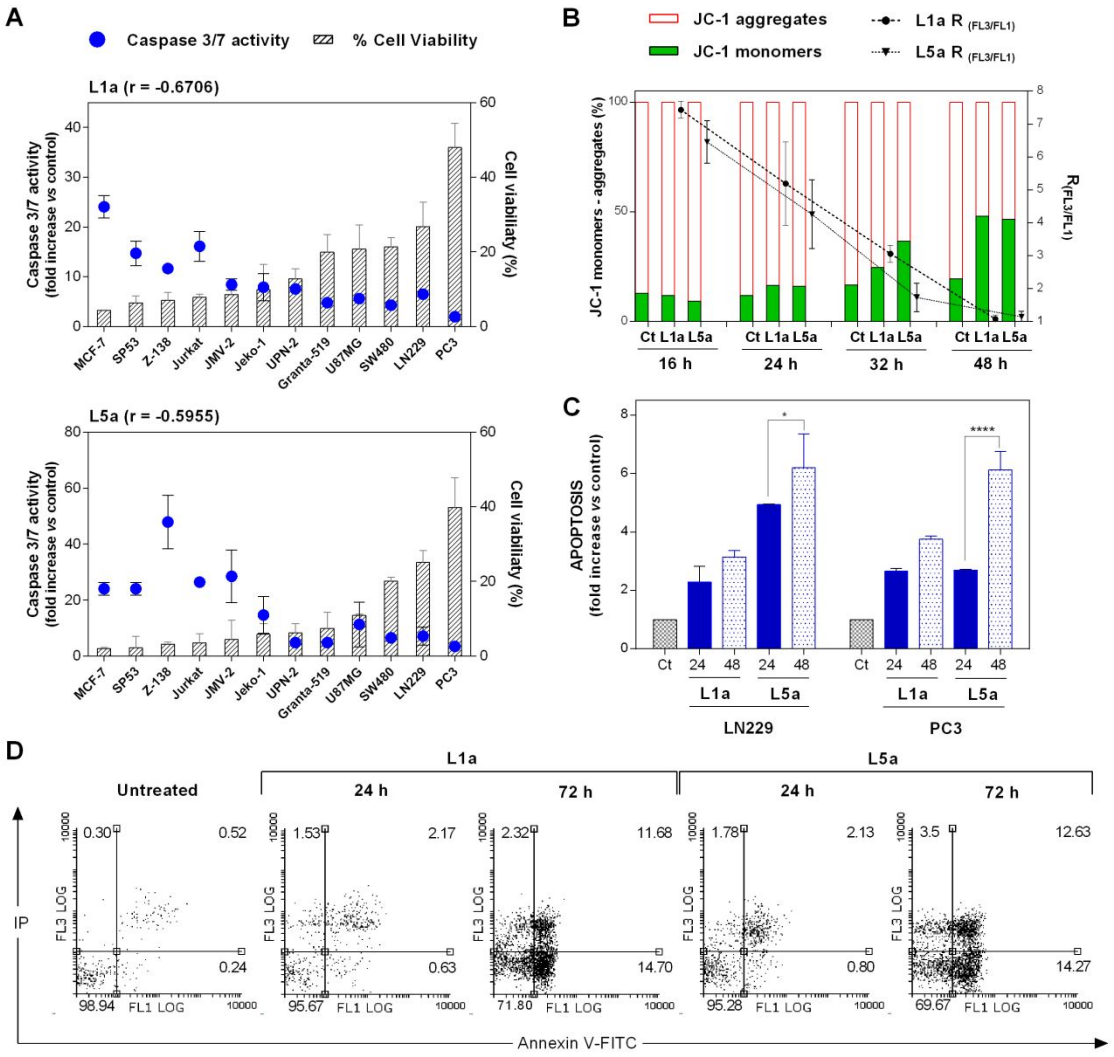

Figure 5. L1a and **L5a** activate the executioner caspases, disrupt the MMP and induce apoptosis. (**A**) Correlation between caspases 3/7 activity (line chart associated with the left y-axis) and cell viability (bar chart associated with the right y-axis). The indicated cell lines were left untreated (control) or were treated for 48 h with 10 μM **L1a** and **L5a**. Caspase 3/7 was measured as indicated in the Experimental Section. The data show the mean ± SD values from three independent experiments, each conducted in triplicate, representing the fold induction in caspase activity and percentage of viable cells, both relative to untreated conditions. Pearson's correlation coefficient (*r*) and *p*-values were calculated for each analysis (**p*<0.05) (**B**) Time course of Mitochondrial Membrane Potential (MMP). LN229 cells were left untreated (control) or were treated with 10 μM **L1a** and **L5a** for the indicated time-points, stained with JC-1 and analyzed by flow cytometry as described in the Experimental Section. Bar chart represents the percentage of JC-1 aggregates and monomers (left y-axis) and the line chart summarizes the mitochondrial depolarization as JC-1 aggregate (red) /JC-1 monomer (green) fluorescence ratio ($R_{(FL3/FL1)}$, right y-axis). Data are presented as the mean ± SD of the ratio from three independent determinations. (**C**) Quantitative analysis of apoptosis assay data. LN229 and PC-3 cells were left untreated or were treated for the indicated time-points with 10 μM **L1a** and **L5a**. Cells were harvested, stained with Annexin V-FITC/Propidium Iodide and analyzed by flow cytometry as described in the Experimental Section. The graph represents the fold increase in apoptotic (early (AV^+, PI^-) and late (AV^+, PI^+)) cells relative to untreated cells at the indicated time-points. Data represent mean ± SD for three independent experiments. Statistical significance between treatment conditions was determined by two-way ANOVA (*p<0.05; ****p<0.0001). (**D**) Representative flow cytometry results obtained in PC3 cell line at the indicated time-points.

profile-anticancer activity of **L1a** and **L5a** is related to the induction of cellular senescence followed by caspase-dependent apoptotic cell death.

Interestingly, although the effect of both compounds in terms of IC_{50} values across the panel of cell lines is very similar, the magnitude of each of these two molecular events is cell line dependent. For instance, the predominant response in LN229 cells is the induction of senescence whereas in PC3 cells the most robust response is the induction of apoptosis.

DNA damage analysis. Polyamine-based compounds are well-known to interact strongly with anionic molecules such as DNA/RNA mainly due to the electrostatic interactions between their positively charge amino groups and nucleic acids backbone at physiological pH.[19] This interaction plays a pivotal role in DNA condensation and aggregation, which could lead to DNA damage under particular conditions.[20] Therefore, in order to assess whether cellular DNA damage is also involved in the cytotoxic effect of compounds **L1a** and **L5a**, we evaluated their ability to induce DNA Double Strand Breaks (DNA-DSBs). We then monitored the levels of the DSB sensor γ-H2AX and performed clonogenic assays in response to treatment with **L1a** and **L5a** (Figure 6).

H2A.X phosphorylation represents an early event in the DNA Damage Response (DDR) against DSB. We used flow cytometry to measure the accumulation of histone H2A.X phosphorylated at Ser-139 (termed γ-H2AX), a well-established readout for the detection of DSBs, since H2A.X becomes rapidly phosphorylated on this residue upon DNA-DSBs.[21] Quantification of γ-H2AX staining after treatment for 4 h with compounds **L1a** (10 μM) and **L5a** (10 μM) revealed that these compounds did not increase H2A.X phosphorylation neither in LN229 cells nor in the more sensitive Z-138 cells, in contrast to the well-established chemotherapeutic agent doxorubicin (Figure 6A,B).

We next investigated whether **L1a** and **L5a** could promote the long-term growth-inhibitory effects elicited by DNA-damaging agents, performing clonogenic assays upon a short exposure to **L1a** and **L5a**. To this end, LN229 and PC-3 cells were treated with **L1a** and **L5a** (10 μM for 4 h) and seeded at low density to follow-up colony formation. The clonogenicity of **L1a**,**L5a**-treated cells was very similar to that of untreated cells, whereas treatment with a standard genotoxic agent such as etoposide dramatically reduced colony formation (Figure 6 C,D).

The absence of H2A.X phosphorylation along with the lack of observed effects in clonogenic assays clearly rule out these compounds as genotoxic agents and thus indicate that **L1a** and **L5a** do not elicit their anticancer effects by promoting cellular DNA damage.

Intracellular zinc measurements: *Zinquin* fluorescence assay. With the goal of better understanding the mechanism of action of **L1a** and **L5a**, we reasoned that these compounds fit with the well-known apoptosis-inducing ability and metal affinity of chelating agents, among which is included the structural class of polyamines.[9b,11-12,13b] Thus, to assess whether the biological effect of **L1a** and **L5a** was due to their chelating properties, we treated LN229 and PC3 cells with compounds **L1a** and **L5a** in the absence or presence of supplemented Zn^{2+}, Cu^{2+}, Fe^{2+} and Fe^{3+} ions in culture medium. As depicted in Figure 7A, addition of exogenous Zn^{2+} and Cu^{2+} ions almost completely counteracted the cellular effect of compounds **L1a** and **L5a** both in LN229 and PC3 cells, whereas the effect of iron resulted in only partial cell growth inhibition (Figure 7A). These observations are in agreement with the hypothesis that zinc chelation, and possibly copper, could be a probable mechanism of **L1a** and **L5a**-induced cytotoxicity. Nevertheless, the results obtained by adding metal ions to cells do not represent a real cellular environment and therefore **L1a** and **L5a** intracellular metal chelation properties. Accordingly, to find out whether **L1a** and **L5a** affect the endogenous levels of metals, a metal-specific assay could be undertaken, specifically the *Zinquin* probe, used to detect and quantify labile intracellular Zn^{2+}. Intracellular "labile" pools of Zn^{2+} include free or loosely bound pools and may even more tightly bound Zn^{2+} populations that are still sensitive to chelation. In contrast, the fixed pools of Zn^{2+} are those that are tightly bound in complexes with high affinity ligands such as in metalloproteins.[22] Regarding intracellular labile copper chelation, it is reasonable to think we could preclude *in vivo* **L1a** and **L5a**-Cu^{2+} interaction as free ionic cytoplasmic copper concentration is extremely low in cells (estimated at <1 ion per cell). Certainly, labile copper concentration is much lower than that of Zn^{2+}, and it is not present to a significant extent.[22a,23] Zn^{2+} is the second most abundant transition metal and the relationship between depletion of labile zinc and the activation of caspase-3 is well described. In addition, zinc depletion is implicated in mitochondrial injury and apoptosis as we observed for **L1a** and **L5a** treatments.[10-11,12c,24]

On the other hand, the metal chelator *N*,*N*,*N*',*N*'-tetrakis(2-pyridylmethyl)ethylenediamine (TPEN), structurally related to the *N*,*N*'-bis(2-pyridylmethyl) polyamines **L1a** and **L5a**, has been reported to induce apoptosis in cancer cells.[11a,12c,12d,13b,22a] TPEN has been shown to trigger cell killing through varied mechanisms attributed to the diverse roles that metals chelated by TPEN play in physiological processes. Furthermore, TPEN has been used mainly as a selective Zn^{+2} chelator, despite the fact that it has a significantly higher affinity for Cu^{+2}.[9b] Thus, **L1a** and **L5a** might behave as pentadentate ligands for transition metal ions through their five nitrogen donor atoms, analogously to TPEN, in which all nitrogen atoms coordinate to zinc.[9b] In addition, the cytotoxicity of TPEN on fibroblasts was compared with that of **L1a** and **L5a** under the same conditions. TPEN IC_{50} value (6.70 ± 2.03 μM) was significantly lower in comparison to **L1a** and **L5a** (29.69 ± 3.92 μM and 20.47 ± 6.08 μM). This result highlights the potential advantage of polyamines **L1a** and **L5a.**

Consequently, in order to assess whether zinc chelation played a role in the observed LN229 and PC-3 cell growth inhibition, we estimated the intracellular labile zinc levels in LN229 glioma cells treated with selected polyamines by fluorescence *in vitro* studies with the membrane-permeant zinc-specific chelator fluorophore *Zinquin*, ethyl (2-methyl-8-*p*-toluenesulphonamido-6-quinolyloxy)acetate (Figure 7B-D). *Zinquin* forms two *Zinquin*:Zn^{2+} complexes with binding constants of $2.7x10^6$ (1:1 complex) and $11.7x10^6$ (2:1 complex). These relatively low affinities for Zn^{2+} ensure

that *Zinquin* preferentially reacts with the most labile Zn^{2+} pools and exclude it from interacting with the tightly bound structural Zn^{2+} in metalloenzymes in a range of cell types.[22a] The *Zinquin* fluorescence assay was performed according to a previously published method.[22b] A decrease of emitted fluorescence by *Zinquin*-Zn^{2+} complex formation was observed

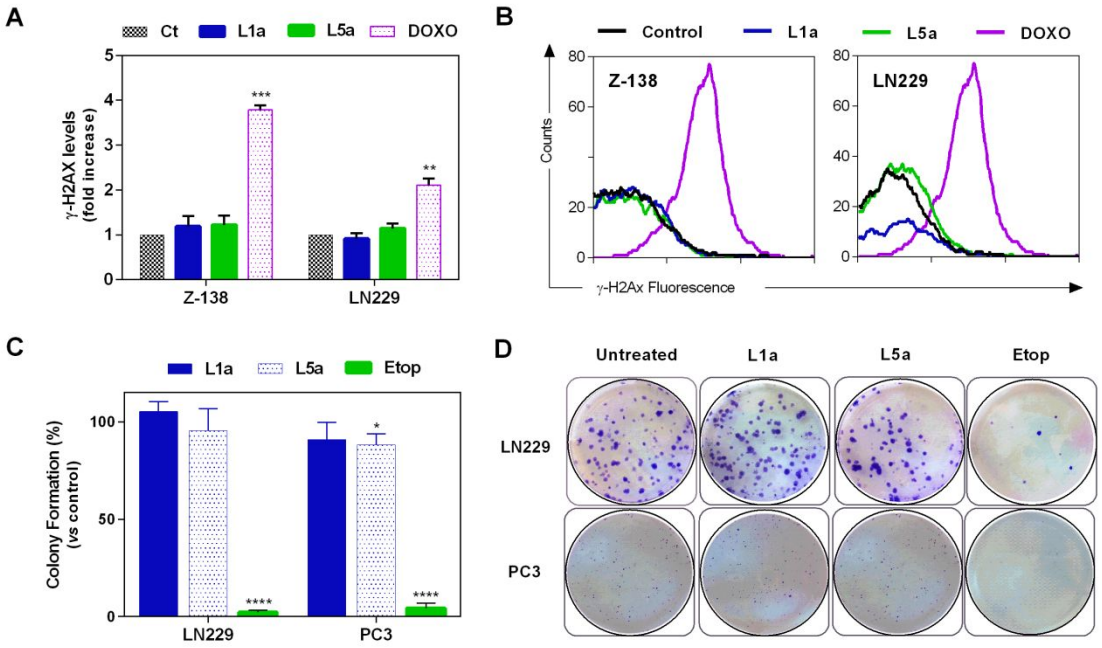

Figure 6. L1a and **L5a** do not induce DNA damage. (**A**) Quantitative analysis of γ-H2AX phosphorylation levels. Z-138 and LN229 cells were left untreated or were treated with **L1a** (10 μM), **L5a** (10 μM) and DOXO (Doxorubicin 1 μM as positive control). After 4 h, the cells were harvested, stained with anti-pS139H2A.X and analyzed by flow cytometry as indicated in the Experimental Section. The graph summarizes the flow cytometry data obtained in all tested cell lines, representing the fold increase in γH2AX positive fluorescence relative to untreated cells (control). The results are expressed as mean ± SD of three independent experiments. Difference from control is sustained by Student's t test (**p<0.01; ***p<0.001). (**B**) Representative histogram profiles corresponding to the above treatments. (**C**) Clonogenic assay. LN229 and PC-3 cells were left untreated (control) or were treated for 4 h with **L1a** (10 μM), **L5a** (10 μM) and Etop (Etoposide 30 μM as positive control) and plated at low density to measure their clonogenic potential as indicated in the Experimental Section. The graph represents the percentage of viable colonies, relative to control. The results are expressed as mean ± SD from four independent experiments each conducted in duplicate. Difference from control is sustained by Student's t test (*p<0.05; **p<0.01; ***p<0.001; ****p<0.0001). (**D**) Representative colony formation images corresponding to the above treatments**.**

in **L1a** and **L5a**-treated cells, indicating that **L1a** and **L5a** do reduce the intracellular concentration of labile zinc ions in LN229 cells in contrast with inactive compounds (Figure 7B). Additionally, the observed intracellular zinc depletion occurred in a dose-dependent manner (Figure 7C). Multiphoton fluorescence microscopy, a well-established imagining technique, confirmed the same marked decrease in fluorescence. Thus, **L1a-L5a** treated cells showed a minimal perinuclear speckled staining pattern in comparison with the densely fluorescence in untreated cells, where the characteristic starry-sky appearance over the whole cytoplasmatic region was observed (Figure 7D). Overall, these results indicate that compounds **L1a** and **L5a** are endowed with a high intracellular zinc chelating capacity in clear correlation with their ability to promote caspase-dependent apoptosis, thus suggesting that **L1a** and **L5a**-mediated cell growth inhibition is mainly associated with the reduction of intracellular zinc levels.

Zinc coordination: potentiometric and quantum mechanical studies. Taking into account the biological results that indicated intracellular Zn^{2+} complex formation as a potential mechanism of **L1a** and **L5a** cytotoxic effect, we evaluated the chelating ability of selected polyamines towards

Zn^{2+} in solution, by studying the coordination mode and the stability constants of Zn^{2+} metal complexes. Metal chelating effect of a ligand requires understanding metal-proton competition for the available basic sites on the ligand as well as the stoichiometry of the complexes formed. Therefore, the potentiometric analysis of polyamines **L1a-c**, **L2a**, **L3a**, **L5a** and **L5c** was performed to determine both their speciation at different pH values, and the stability constants of the corresponding Zn^{2+} metal complexes. The selection of polyamines under study was carried out to illustrate the main features of structural diversity according to ligand's functionalization as well as pyridinic nitrogen positions. Protonation and complex formation equilibrium studies were carried out under the same conditions described in previous publications.[15,25]

Prior to studying Zn^{2+}-polyamine complexation, the protonation constants were calculated by potentiometric measurements in the pH range 2.0-11.5 at 298.1 K with 0.15 M NaCl ionic strength. The data were processed using the HYPERQUAD program,[26] and the protonation constants and the distribution diagrams are reported in ESI (Table S4.1 and Figures S4.1-S4.6).

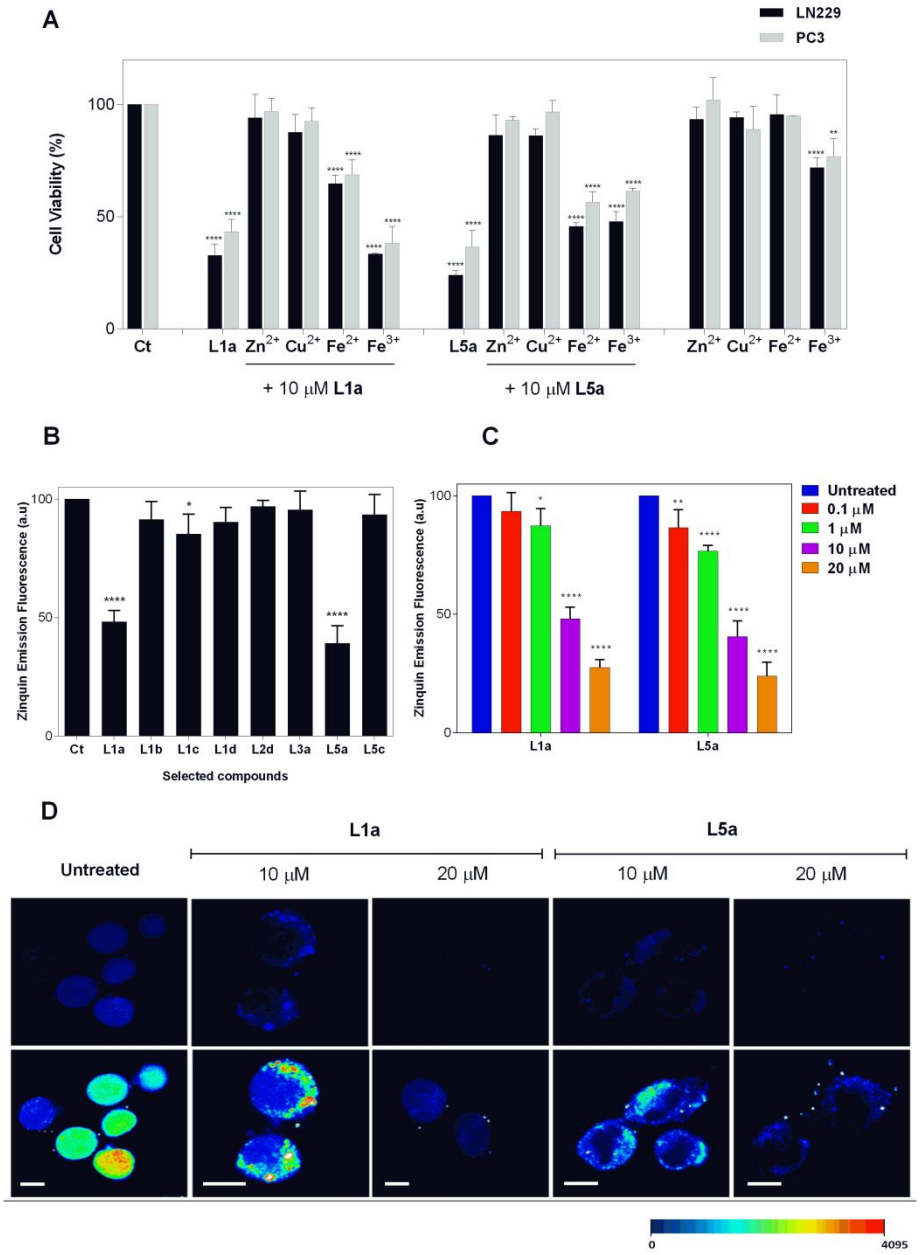

Figure 7. Metal chelating properties of **L1a** and **L5a**. (**A**) The indicated cell lines were treated for 48 h with 10 μM L1a or L5a, with the corresponding chloride (15 μM): $ZnCl_2$ (Zn^{2+}), $CuCl_2$ (Cu^{2+}), $FeCl_2$ (Fe^{2+}), $FeCl_3$ (Fe^{3+}), or with their association. The mean ± SD values from three independent experiments each conducted in triplicate are shown in the graph, representing the percentage of viable cells relative to untreated conditions. Statistical significance between treatment conditions was determined by one-way ANOVA (*p<0.05; **p<0.01; ***p<0.001; ****p<0.0001). (**B**), (**C**) and (**D**) Detection of intracellular labile zinc by *Zinquin* assay. LN229 cell line was left untreated (control) or was treated with **L1a** and **L5a** for 12 h. *Zinquin* assay was performed as indicated in the Experimental Section. Fluorescence signal in each sample was normalized according to its own cell number, and signal from untreated cells was set to 100. Data represent mean ± SD for four independent experiments. (**B**) and (**C**) Emission fluorescence quantification at 475 nm in treated LN229 cells with the selected compounds. (**D**) Representative Zn-dependent *Zinquin* multiphoton microscope images in LN229 cells. Upper panel show the obtained raw images and the lower panel shows pseudo-colored images for better visualization. Scale bar = 10 μm.

Subsequently, the complex formation equilibrium between Zn^{2+} and **L1a-c**, **L2a**, **L3a**, **L5a** and **L5c** was studied potentiometrically. The stability constant values are reported in Table 1 and the distribution diagrams in Figure 8 and the ESI (Figures S5.1- S5.2). Potentiometric studies of the binary Zn^{2+}-L systems showed the formation of 1:1 complex for all the compounds. We observed the formation of mononuclear $[ZnL]^{2+}$ species for **L1a**, **L5a** and **L5c**. In addition, variously protonated 1:1 $[ZnH_rL]^{(2+r)+}$ complexes with r = 1 – 0 for **L1b** and **L1c** and r = 2 – 0 for **L2a** were characterized. We also detected one monohydroxylated species

Table 1. Logarithms of the stability constants for the formation of Zn^{2+} complexes determined at 298.1 K in 0.15 M NaCl. Determined in 0.15 NaCl at 298.1 + 0.1 K in aqueous solutions for L1b, L1c, L2b and L3a, or hydroalcoholic solutions (H_2O:EtOH 70:30) for L5a and L5c.

Reaction[a]	Log K[e]						
	L1a[b]	**L1b**	**L1c**[c]	**L2a**[d]	**L3a**	**L5a**	**L5c**
$Zn + L + 2H \leftrightarrows ZnH_2L$				17.49(6)			
$Zn + L + H \leftrightarrows ZnHL$	16.66	14.12(3)		12.99(6)			
$Zn + L \leftrightarrows ZnL$	13.01(2)	6.04(3)	4.72(1)	8.38(4)	7.53(1)	13.40(2)	6.57(1)
$Zn + L + H_2O \leftrightarrows ZnL(OH) + H$	2.25(3)	-2.56(2)	-4.22(2)	-1.17(5)	-1.48(1)	2.81(4)	-2.6(3)
$Zn + L + 2H_2O \leftrightarrows ZnL(OH)_2 + 2H$		-12.10(2)	-12.89(1)	-11.54(4)	-11.77(1)		-12.28(2)
$ZnL + H_2O \leftrightarrows ZnL(OH) + H$	-10.76(3)	-8.60(2)	-8.99(2)	-9.55(4)	-10.01(1)	-10.59(4)	-9.17(3)
$ZnL(OH) + H_2O \leftrightarrows ZnL(OH)_2 + H$		-9.54(2)	-8.67(2)	-10.37(5)	-10.29(1)		-9.68(3)
$ZnHL + H \leftrightarrows ZnH_2L$				4.50(6)			
$ZnL + H \leftrightarrows ZnHL$	3.65(3)			4.61(2)			
$2L + Zn + 2H \leftrightarrows ZnH_2L_2$							24.31(3)

[a]Charges omitted. [b]Taken from ref. 25b. [c]Taken from ref. 15. [d]Taken from ref. 25a. [e]Values in parentheses are standard deviations in the last significant figure.

$[ZnL(OH)]^{3+}$ for all the compounds and even dihydroxylated species $[ZnL(OH)_2]^2$ for **L1b, L1c**, **L2a, L3a** and **L5c**. We then analyzed the stability constants of Zn^{2+} complexes (Table 1). It is important to note significant differences in the complex formation equilibria. Thus, the stability constants of the mononuclear equilibrium (Zn^{2+} + L = ZnL^{2+}) for compounds containing 2-pycolyl substituents are higher than the ones containing 3- and 4-pycolyl moieties, i.e. **L1a** in comparison with **L1b** and **L1c**. Within this series of compounds, the stability constant for the Zn**L1a**$^{2+}$ complex is 13.01 logarithmic units while for **L1b** and **L1c** the values are 6.04 and 4.72 respectively, which implies a decrease of the constant values more than 7 orders of magnitude.

Similarly, when we compared **L5a** and **L5c** constant values, a stability constant of 13.4 was obtained for **L5a**, while a lower value of 6.57 was determined for **L5c**. Taking into account these values, the higher affinity of **L1a** and **L5a** could be attributed to the effective chelating contribution of the pyridine ring nitrogens at *orto* position to form a Zn^{2+} coordinate bonds that enables the ligands to stabilize the Zn^{2+} complexes. Therefore, it can be suggested that metal coordination in ZnL^{2+} 2-pyridyl substituted **L1a** and **L5a** species involves the three nitrogen atoms of the polyamine chain along with the heterocyclic nitrogen atoms. While, the binding of the two secondary amino groups of the polyaminic chain is exclusively involved in 3- and 4-pycolyl substituted Zn**L1b**$^{2+}$, Zn**L1c**$^{2+}$ and Zn**L5c**$^{2+}$ species. With regard to the other 2-pycolyl derivatives **L2a** and **L3a**, we observed lower stability constants (log K 8.38 and 7.53, respectively) in comparison with **L1a** and **L5a**, probably due to the electron-withdrawing character of the sulfonyl moiety that decreases the coordination ability of the central amino group.

These results were further confirmed by quantum mechanical (QM) studies (Figure 8 and Figures S6.1-S6.7). The minimum energy conformations of Zn**L1a**$^{2+}$and Zn**L5a**$^{2+}$ complexes indicated Zn^{2+} coordination through the nitrogen atoms of the polyamine chain along with the pyridine nitrogens. However, the Zn^{2+} coordination sphere in **L1b** and **L1c** involves exclusively the aliphatic nitrogen atoms completed with solvent molecules (Figure 8). Concerning to **L1d**, we could not detect by potentiometry the formation of any Zn^{2+} complex in the studied pH range, although QM studies indicated a Zn^{2+} coordination sphere in which all the nitrogen atoms coordinate the metal similarly to the structural analogue **L1a**. Nevertheless, in comparison with **L1a**, the poor donor character of the amide nitrogens in **L1d** is observed by the lengthening of Zn-N2 and Zn-N4 distances, increased from 2.255 to 3.025 Å and from 2.205 to 2.299 Å, respectively (Figure S6.1 and Figure S6.5). In addition, a similar coordination sphere of the metal has

been previously described for analogous compounds to **L1d**.[29] Lengthening of the metal bonding is also observed in the Zn**L2a**$^{2+}$ complex by QM studies. Thus, the minimum energy Zn**L2a**$^{2+}$ conformer showed, in comparison to **L1a**, an increasing in the distance Zn–N3 from 2.314 to 3.096 Å caused by the substitution of the naphthylmethyl moiety by the sulfonyl scaffold (Figure S6.6).

Additionally, we can observe in Figure 8 that **L1a** and **L5a,** compounds containing the 2-pyridyl substitution, showed fully Zn^{2+} complexation (>99%) at physiological pH

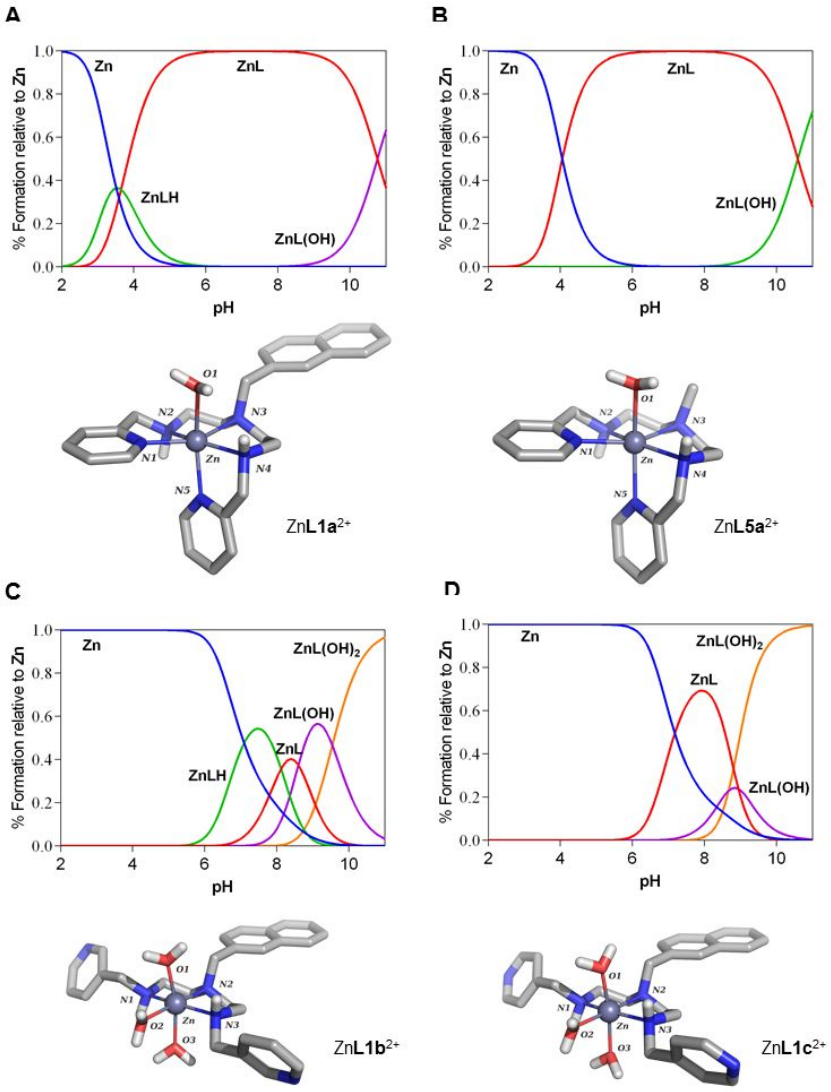

Figure 8. Distribution diagrams of Zn^{2+}-L (**A: L1a; B: L5a; C: L1b; D: L1c**) complex formation and QM models of their optimized geometry**.**

7.4, whereas the percentage of complexed metal was lower for the 3- and 4-pyridyl substituted compounds **L1b** and **L1c** (63.4% and 60.7%, respectively).

SAR analysis. In accordance with the biological and metal coordination results of polyamines **L1**-**L5**, a precise Structure-Activity Relationship (SAR) could be defined as shown in Figure 9.

i) Sulfonamide and carboxamide linkages resulted in complete abolition of the antiproliferative efficacy. Thus, the biological activity is completely dependent on the architecture of the polyamine backbone, since the replacement of the two inner amine functions of polyamine **L1a** into carboxamide moieties affording the corresponding polyamine **L1d**, altered dramatically the cytotoxicity. Analogously the substitution of the naphthylmethyl group or methyl group by an arylsulfonyl moiety resulted in a complete loss of cytotoxicity. Indeed, polyamines **L1a** (naphthylmethyl) and **L5a** (methyl) showed higher antiproliferative activities than their sulfonylated counterparts **L2a**, **L3a** or **L4a**. Thus, the introduction of carbonyl and/or sulfonyl groups hampers the nitrogen to participate in metal coordination at neutral pH, and consequently the antiproliferative effect is depleted, confirming the involvement of the amines in zinc coordination and cytotoxicity.

ii) Concerning the nitrogen atom position onto the pyridine ring, we observed by comparing the cytotoxic efficacy obtained with polyamines **L1a-c** and **L5a,c**, that the nitrogen atom insertion in 3- or 4- position of the aromatic heterocyclic rings can be found in compounds lacking antiproliferative activity (**L1b**, **L1c** and **L5c**). Whereas compounds **L1a** and **L5a** with 2-pyridyl substituents show the highest cytotoxic activity. This finding suggests the crucial role of the nitrogen heteroatom in 2-position onto the terminal pyridine rings, since it gives rise to more stable complexes with the metal ion, in accordance with the coordination and computational studies.

Taking the above-mentioned molecular features into account, we could assume that the pharmacophore of our small library would be defined by a 1,7-bis-2-picolyl-1,4,7-triazaheptane framework, conveniently substituted onto the central nitrogen. It is important to note that the well-studied polyazaalkane scaffold containing 2-picolyl subunits is a structural motif frequently used as building block of biologically relevant molecular receptors, which interact with both cationic and anionic ions. In this line, structurally similar Zn^{2+} and Cu^{2+} receptors have been described as chelating agents,[8c,9b,30] mechanism whereby they mediate their anticancer activity in different cancer cell lines, or biosensors for anions through specific recognition of phosphate-containing biomolecules or mononucleotides.[31]

Therefore, our SAR findings are consistent with the use of an appropriate polyamine backbone as template, bearing a penta-nitrogenated framework where the electron donor character of the nitrogen atoms seems to play an important role participating in zinc metal binding, which might be useful for the antiproliferative efficacy.

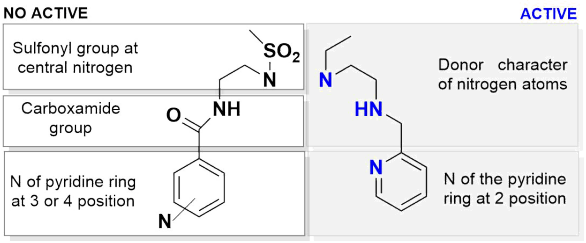

Figure 9. SAR analysis of antiproliferative activity of polyamines **L1-L5.**

ADME *in silico* evaluation. Finally, having established the biological activity of compounds **L1a** and **L5a**, we evaluated the physicochemical properties, pharmacokinetics and drug-likeness using the SwissADME online toolkit[32] (Table 2). According to this model, both compounds showed satisfactory oral bioavailability as the combination of the main six descriptors (lipophilicity, molecular weight, polarity, solubility, saturation and flexibility) ranged inside the acceptable radar plots (Figure S7.1). Moreover, the drug-likeness of **L1a** and **L5a** was also evaluated by the number of free rotatable bonds (n-ROTB) and Lipinski's as well as Veber's, Egan's and Muegge's rules[32]. Although **L5a** showed better drug-likeness and pharmacokinetic profiles in comparison to **L1a**, both compounds in general fulfilled the criteria, an important characteristic for future drug development.

CONCLUSIONS

In summary, we have shown that it is possible to design linear symmetrically substituted polyamine derivatives with high *in vitro* cytotoxic activity against a broad panel of human cancer cell lines of different origin.

The anticancer activity evaluation of our library of polyamines **L1-L5** allowed the identification of 2-pyridyl derivatives **L1a** and **L5a** as novel polyamine-based pharmacologically active molecules, with significant *in vitro* growth inhibitory efficacy, validated in 14 human cancer cell lines of different origin. The structural similarity between both compounds has enabled to establish a SAR approach, identifying the bis-2-picolyldiethylentriamine scaffold as a pharmacophoric element for the cytotoxic profiles. Importantly, both compounds **L1a** and **L5a** induced G1 cell cycle arrest followed by senescence and apoptosis in LN229 and PC3 cells, in the absence of cellular DNA damage. Another encouraging finding was the observation of the zinc-chelator critical role of **L1a-L5a** for the cytotoxic activity, evidenced by the specific *Zinquin* assay and Zn^{2+} coordination studies. This result suggests intracellular Zn^{2+} depletion as a potential target of polyamines **L1a** and **L5a** necessary for cancer cell cytotoxicity.

Overall, our studies provide significantly important results for the lead optimization process and the development of a novel type of antineoplastic drugs readily accessible. Further details on the precise mechanism of action and *in vivo* experiments are currently under study in our laboratory.

Table 2. Selected physicochemical descriptors and drug-likeness and pharmacokinetic parameters of L1a and L5a.

	L1a	**L5a**
Physicochemical Properties		
Molecular weight	426.58 g/mol	300.42 g/mol
Num. rotatable bonds	12	10
Num. H-bond acceptors	4	4
Num. H-bond donors	2	2
TPSA	57.66 Å²	57.66 Å²
Lipophilicity		
Consensus Log $P_{o/w}$	2.51	0.45
Drug-likeness (no. of violations)		
Lipinski	Yes (0)	Yes (0)
Veber	Yes (1)	Yes (0)
Egan	Yes (0)	Yes (0)
Muegge	Yes (0)	Yes (0)
Bioavailability Score	0.55	0.55
Pharmacokinetics		
GI absorption	High	High
BBB permeant	Yes	No
CYP1A2 inhibitor	Yes	No
CYP2C19 inhibitor	No	No
CYP2C9 inhibitor	No	No
CYP2D6 inhibitor	No	No
CYP3A4 inhibitor	Yes	No

EXPERIMENTAL

Chemistry general. All reagents and solvents were purchased from commercial sources and were used without further purification. Reactions requiring anhydrous conditions were carried out under nitrogen atmosphere. Anhydrous solvents were purified using an MBRAUN solvent purification system MB SPS-800 Series (MBRAUN SPS Systems). To obtain hydrochloride salts, it was used dry ethanol from secure sealed bottles (Seccosolv®, max. 0.01 % H_2O). Thin-Layer Chromatography (TLC) was carried out on aluminum oxide or silica gel pre-coated plates (60 PF254, Merck). Detection of the compounds was achieved by fluorescence quenching at 254 nm or staining with ninhydrin (0.3 % ethanolic solution). Column chromatography purifications were performed on neutral aluminium oxide or silica gel 60 (0.040–0.063 mm) from Merck. The intracellular zinc chelator *N*,*N*,*N*',*N*'-tetrakis (2-pyridylmethyl) ethylenediamine (TPEN) was obtained from Sigma (St. Louis, MO). Melting points were determined in open capillary tubes using a SMP3 Stuart™ melting point apparatus (Bibby) and are uncorrected. 1D (^{1}H, ^{13}C, DEPT) and 2D (COSY, HSQC) NMR spectra were recorded at room temperature on a Bruker Advance DPX300 spectrometer operating at 299.95 MHz for ^{1}H and 75.43 MHz for ^{13}C and referenced to tetramethylsilane (TMS) or 3-(trimethylsilyl) propionic-2,2,3,3-d4 (TSP) acid sodium salt. Chemical shifts (δ values) and coupling constants (*J* values) are given in ppm and Hz respectively. High resolution mass spectrometry (HR-MS) was performed with electron spray ionization (ESI) recorded on an Esquire 300 (Bruker) by electrospray positive mode (ES+) or negative modes (ES-). Elemental analysis was performed with a CE Instruments EA1110 CHNS-O equipment. Purity of the compounds (≥95%) and molecular mass were confirmed by HRMS and elemental microanalysis. The analytical results for C, H, N and S were within ± 0.4 of the theoretical values.

The purity of active compounds was determined by HPLC and was confirmed to be ≥95%. The instrument used was a Water ACQUITY® TQD separation module using a Hydrosphere C18 BEH column (2.1 mm × 50 mm, 1.7 µm) with water containing 0.1% formic acid as solvent A and methanol as solvent B at a flow rate of 0.4 mL/min and column temperature, 30 °C. The gradient program was as follows: 5% B (0–2 min), 5–95% B (2–6.5 min), and 95-5% B (6.5–10 min).

Synthesis of 3-*N*-substituted 1,5-diphthalimido-3-azapentanes L(1-4)-ft. The synthesis of the starting material diphthalimido-3-azapentane **L-ft** was carried out as described elsewhere.[33] Compounds **L1-ft** and **L2-ft** were synthesized following the general procedure described in reference 15.

3-(1-Naphthylsulfonyl-)-1,5-diphthalimido-3-azapentane (L3-ft). Diphthalimido-3-azapentane **L-ft** (0.67 g,1.85 mmol), 1-naphthalenesulfonyl chloride (0.67 g, 2.96 mmol) and K_2CO_3 (0.5 g, 3.62 mmol) were dissolved in MeCN (300 mL) and the reaction mixture was refluxed for 24 h under nitrogen atmosphere. After filtration, the solvent was removed under reduced pressure. The resulting residue was mixed with water (100 mL) and extracted with CH_2Cl_2 (3 x 50 mL). The organic phase was dried over Na_2SO_4, filtered and concentrated under reduced pressure. The residue was recrystallized from EtOH to give pure **L3-ft** as a white solid. Yield 0.93 g (91%); mp 206-208 ºC; ^{1}H NMR (300 MHz, DMSO-d_6) δ 3.81 (s, 8H), 7.18 (ddd, *J* = 8.2, *J* = 6.9, *J* = 1.0, 1H), 7.41 (ddd, *J* = 8.7, *J* = 6.9, *J* = 1.4, 1H), 7.44 (dd, *J* = 8.2, *J* = 7.4, 1H), 7.48 (d, *J* = 8.2, 1H), 7.61-7.64 (m, 4H), 7.72-7.75 (m, 4H), 7.84 (d, *J* = 8.2, 1H), 7.96 (dd, *J* = 7.4, *J* = 1.2, 1H), 7.95 (dd, *J* = 8.7, *J* = 1.0, 1H); ^{13}C NMR (75 MHz, DMSO-d_6) δ 34.6 (CH_2), 42.5 (CH_2), 123.3 (CH), 123.8 (CH), 124.5 (CH), 126.8 (CH), 127.1 (C), 128.2 (CH), 129.1 (CH), 130.4 (CH), 131.6 (C), 133.6 (C), 133.7 (C), 134.4 (CH), 134.63 (CH), 167.82 (C=O); HRMS (ESI+) *m/z* [M + H] calcd for $C_{30}H_{24}N_3O_6S$: 554.1380, found: 554.1398.

3-(8-Quinolylsulfonyl-)-1,5-diphthalimido-3-azapentane (L4-ft). L-ft (0.65 g, 1.78 mmol), 8-quinolinesulfonyl chloride (0.65 g, 2.85 mmol) and K_2CO_3 (0.5 g, 3.62 mmol) were dissolved in MeCN (300 mL) and the reaction mixture was refluxed for 24 h under nitrogen atmosphere. After filtration, the solvent was removed under reduced pressure. The resulting residue was mixed with water (100 mL) and extracted with CH_2Cl_2 (3 x 50 mL). The organic phase was dried over Na_2SO_4, filtered and concentrated under reduced pressure. The residue was recrystallized from EtOH to give pure **L4-ft** as a white solid. Yield 0.66 g (67%); mp 229-230 ºC; ^{1}H NMR (300 MHz, DMSO-d_6) δ 3.79 (t, *J* = 5.7, 4H), 3.99 (t, *J* = 5.7, 4H), 7.39-7.43 (m, 2H), 7.56-7.60 (m, 4H), 7.70 (dd, *J* = 8.3, *J* = 1.5, 1H), 7.72-7.77 (m, 4H), 7.96 (dd, *J* = 8.3, *J* = 1.8, 1H), 8.05 (dd, *J* = 7.3, *J* = 1.5, 1H), 8.88 (dd, *J* = 4.2, *J* = 1.8, 1H); ^{13}C NMR (75 MHz, DMSO-d_6) δ 34.9 (CH_2), 43.6 (CH_2), 122.4 (CH), 123.3 (CH), 125.4 (CH), 128.4 (C), 131.5 (C), 131.7 (CH), 133.7 (CH), 134.3 (CH), 136.7 (CH), 137.5 (C), 142.6 (C), 151.4 (CH), 167.8 (C=O); HRMS (ESI+) *m/z* [M + H] calcd for $C_{29}H_{23}N_4O_6S$: 555.1333, found: 555.1357.

Synthesis of 4-*N*-substituted 1,4,7-triazaheptane compounds (L1-4)

The corresponding polyamine **L(1-4)-ft** (1 equiv) and hydrazine monohydrate (20 equiv) were dissolved in EtOH (400 mL) and the reaction mixture was refluxed for 24 h under nitrogen atmosphere. The precipitate was removed by filtration and the solvent was evaporated under vacuum. The resulting oil was dissolved in $CHCl_3$ (300 mL) and the solution was stirred for 24 h under nitrogen. After filtration, the solvent was evaporated to dryness to give an oily product, which was characterized as the corresponding amine **L1**, **L2**, **L3** or **L4**. Compounds **L1** and **L2** were synthesized following the general procedure described in references 15 and 25a, respectively.

4-(1-Naphthylsulfonyl-)-1,4,7-triazaheptane (L3). Following the general procedure described above, compound **L3** was prepared from **L3-ft** (0.53 g, 0.96 mmol). Yield 0.21 g (75%); ^{1}H NMR (300 MHz, $CDCl_3$) δ 2.33 (t, *J* = 6.4, 4H), 3.34 (t, *J* = 6.4, 4H), 7.53 (dd, *J* = 8.3, *J* = 7.4, 1H), 7.60 (ddd, *J* = 8.3, *J* = 6.9, *J* = 1.3, 1H), 7.66 (ddd, *J* = 8.6, *J* = 6.9, *J* = 1.5, 1H), 7.93 (dd, *J* = 8.3, *J* = 1.1, 1H), 8.06 (d, *J* = 8.3, 1H), 8.21 (dd, *J* = 7.4, *J* = 1.3, 1H), 8.66 (dd, *J* = 8.6, *J* = 1.1, 1H); ^{13}C NMR (75 MHz, $CDCl_3$) δ 40.8 (CH_2), 51.4 (CH_2), 124.5 (CH), 125.1 (CH), 127.3 (CH), 128.6 (CH), 129.0 (C), 129.5 (CH), 130.1 (CH), 134.7 (CH), 134.8 (C), 134.9 (C).

4-(8-Quinolylsulfonyl-)-1,4,7-triazaheptane (**L4**). Following the general procedure described above, compound **L4** was prepared from **L4-ft** (0.51 g, 0.92 mmol).

Yield 0.20 g (76%); ^{1}H NMR (300 MHz, $CDCl_3$) δ 1.68 (b.s, 4H, NH), 2.79 (t, *J* = 6.4, 4H), 3.42 (t, *J* = 6.4, 4H), 7.45 (dd, *J* = 8.3, *J* = 4.2, 1H), 7.54 (t, *J* = 7.8, 1H), 7.95 (d, *J* = 8.2, 1H), 8.16 (dd, *J* = 8.3, *J* = 1.5, 1H), 8.44 (dd, *J* = 7.8, *J* = 1.4, 1H), 8.98 (dd, *J* = 4.2, *J* = 1.5, 1H); ^{13}C NMR (75 MHz, $CDCl_3$) δ 40.2 (CH_2), 51.7 (CH_2), 121.1 (CH), 124.5 (CH), 128.0 (CH), 132.4 (CH), 132.5 (C), 135.6 (CH), 136.4 (C), 142.9 (C), 150.1 (CH).

Synthesis of polyamines L1a-c, L2(a,b), L3a, L4a, and L5(a,c). The corresponding pyridinecarboxaldehyde (2.1 equiv) dissolved in EtOH (100 mL) was added dropwise to a solution of 4-*N*-substituted amine precursor **L1-4** or the commercially available amine 4-methyl-1,4,7-triazaheptane **L5** (1 equiv) in EtOH (50 mL). The reaction mixture was stirred at room temperature under nitrogen atmosphere for 4 h. $NaBH_4$ (10 equiv) was then added portion wise. The mixture was stirred for 6-12 h and the solvent was then vacuum-evaporated to dryness. The residue was treated with water (100 mL) and extracted with CH_2Cl_2 (3 x 50 mL). The organic phase was washed with brine, dried with anhydrous Na_2SO_4, filtered, and the solvent evaporated to dryness. The residue was purified by column chromatography on silica gel or aluminum oxide to give colorless oil. The resulting oil was dissolved in the minimum of dry EtOH or CH_2Cl_2 and the amine was precipitated as its hydrochloride salt with 4 M HCl/dioxane solution (3 mL). Compounds (**L1a·5HCl**), (**L1c·5HCl**) and (**L2a·5HCl**) were synthesized following the procedures described in references 15 and 25.

1,7-Bis(3-pyridylmethyl)-4-(2-naphthylmethyl)-1,4,7-triazaheptane pentahydrochloride (**L1b·5HCl**). **L1** (1.52 g, 6.2 mmol) was reacted with 3-pyridinecarboxaldehyde (1.47 g, 13.7 mmol) according to the general procedure described above to give a yellow oil, which was then precipitated as its pentahydrochloride salt. Yield 1.83 g (69%); mp 181-182 °C; ^{1}H NMR (300 MHz, D_2O) δ 3.28-3.90 (m, 8H), 4.07 (s, 2H), 4.38 (s, 4H), 7.51 (dd, *J* = 8.5, *J* = 1.8, 1H), 7.52-7.57 (m, 3H), 7.81-7.86 (m, 3H), 8.00 (ddd, *J* = 8.1, *J* = 6.0, *J* = 0.7, 2H), 8.55 (td, *J* = 8.1, *J* = 1.8, 2H), 8.75 (d, *J* = 6.0, 2H), 8.79 (d, *J* = 1.8, 2H); ^{13}C NMR (75 MHz, D_2O) δ 44.7 (CH_2), 47.4 (CH_2), 50.8 (CH_2), 59.4 (CH_2), 127.4 (CH), 127.7 (CH), 128.1 (CH), 128.2 (CH), 128.2 (CH), 129.1 (CH), 129.4 (CH), 130.2 (CH), 131.0 (C), 132.9 (C), 133.1 (C), 133.2 (C), 142.5 (CH), 142.6 (CH), 148.5 (CH); HRMS (ESI+) *m/z* [M + H] calcd for $C_{27}H_{32}N_5$: 426.2652, found: 426.2662. Anal. Calcd for $C_{27}H_{36}Cl_5N_5(H_2O)_2$: C, 50.36; H, 6.26; N, 10.87, found: C, 50.35; H, 6.04; N, 10.62.

1,7-Bis(3-pyridylmethyl)-4-(dansyl)-1,4,7-triazaheptane pentahydrochloride (**L2b·5HCl**). **L2** (0.55 g, 1.63 mmol) was reacted with 3-pyridinecarboxaldehyde (0.38 g, 3.6 mmol) according to the general procedure described above to give a light green oil, which was then precipitated as its pentahydrochloride salt. Yield 0.71 g (84%); mp 198-200 °C; ^{1}H NMR (300 MHz, D_2O) δ 3.53 (s, 6H), 3.61 (t, *J* = 6.2, 4H), 3.95 (t, *J* = 6.2, 4H), 4.66 (s, 4H), 7.91–7.93 (m, 2H), 8.14 (d, *J* = 7.8, 1H), 8.20 (d, *J* = 6.1, 1H), 8.22 (d, *J* = 6.4, 2H), 8.53 (d, *J* = 8.7, 1H), 8.81-8.87 (m, 3H), 8.93 (d, *J* = 6, 2H,), 9.05 (d, *J* = 2, 2H); ^{13}C NMR (75 MHz, D_2O) δ 47.2 (CH_3), 47.3 (CH_2), 47.4 (CH_2), 47.8 (CH_2), 120.3 (CH), 126.5 (C), 126.7 (CH), 127.0 (CH), 127.4 (CH), 128.3 (CH), 128.9 (CH), 129.3 (CH), 129.4 (C), 131.4 (C), 134.0 (C), 139.7 (C), 143.0 (CH), 143.1 (CH), 148.7 (CH); HRMS (ESI+) *m/z* [M + H] calcd for $C_{28}H_{36}N_6O_2S$: 519.2537, found: 519.2550. Anal. Calcd for $C_{28}H_{39}Cl_5N_6O_2S(H_2O)_3$: C, 44.54; H, 6.01; N, 11.13; S, 4.25, found: C, 44.66; H, 6.21; N, 11.05; S, 3.79.

1,7-Bis(2-pyridylmethyl)-4-(1-naphthylsulfonyl)-1,4,7-triazaheptane tetrahydrochloride (L3a·4HCl). L3 (1.0 g, 3.4 mmol) was reacted with 2-pyridinecarboxaldehyde (0.80 g, 7.5 mmol) according to the general procedure described above. The residue was purified by column chromatography on neutral aluminum oxide ($CHCl_3$/MeOH 85:15) to give a light brown oil, which was then precipitated as its tetrahydrochloride salt. Yield 0.73 g (45 %); mp 198-200 °C; ^{1}H NMR (300 MHz, D_2O) δ 3.25 (t, *J* = 6.5, 4H), 3.76 (t, *J* = 6.5, 4H), 4.40 (s, 4H), 7.52-7.69 (m, 7H), 7.98 (dd, *J* = 7.6, *J* = 1.7, 1H), 8.06 (dd, *J* = 7.5, *J* = 1.7, 1H), 8.08 (td, *J* = 7.8, *J* = 1.7, 2H), 8.15 (d, *J* = 8.3, 1H), 8.42 (dd, *J* = 8.3, *J* = 1.3, 1H), 8.56 (ddd, *J* = 5.3, *J* = 1.7, *J* = 0.9, 2H); ^{13}C NMR (75 MHz, D_2O) δ 45.1 (CH_2), 45.5 (CH_2), 49.6 (CH_2), 123.3 (CH), 124.5 (CH), 125.4 (CH), 125.8 (CH), 127.4 (C), 127.6 (CH), 129.2 (CH), 129.7 (CH), 129.8 (CH), 131.2 (C), 134.2 (C), 136.0 (CH), 141.8 (CH), 147.1 (CH), 147.6 (C); HRMS (ESI+) *m/z* [M + H] calcd for $C_{26}H_{30}N_5O_2S$: 476.2115, found: 476.2124. Anal. Calcd for $C_{26}H_{33}Cl_4N_5O_2S$: C, 50.25; H, 5.35; N, 11.27; S, 5.16, found: C, 50.08; H, 5.88; N, 11.41; S, 5.35.

1,7-Bis(2-pyridylmethyl)-4-(8-quinolylsulfonyl-)-1,4,7-triazaheptane pentahydrochloride (**L4a·5HCl**). **L4** (1.2 g, 4.1 mmol) was reacted with 2-pyridinecarboxaldehyde (0.96 g, 9 mmol) according to the general procedure described above. The residue was purified by column chromatography on neutral aluminum oxide ($CHCl_3$/MeOH 65:35) to give a pale brown oil, which was then precipitated as its pentahydrochloride salt. Yield: 0.82 g (42%); mp 201-203 °C; ^{1}H NMR (300 MHz, D_2O) δ 3.47 (t, *J* = 6.2, 4H), 3.80 (t, *J* = 6.2, 4H), 4.68 (s, 4H), 7.74-7.77 (m, 2H), 7.94 (ddd, *J* = 7.9, *J* = 5.7, *J* = 1.2, 2H), 8.05 (d, *J* = 7.9, 2H), 8.28 (dd, *J* = 8.4, *J* = 1.4, 1H), 8.48 (m, 3H), 8.65 (dd, *J* = 8.4, *J* = 1.7, 1H), 8.75 (ddd, *J* = 5.7, *J* = 1.7, *J* = 0.7, 2H), 8.97 (dd, *J* = 4.8, *J* = 1.7, 1H); ^{13}C NMR (75 MHz, D_2O) δ 46.4 (CH_2), 46.9 (CH_2), 47.9 (CH_2), 123.1 (CH), 127.1 (CH), 127.5 (CH), 127.6 (CH), 129.6 (C), 130.0 (C), 135.3 (CH), 136.4 (CH), 139.3 (C), 142.4 (CH), 144.1 (CH), 145.1 (C), 146.4 (CH), 150.4 (CH). HRMS (ESI+) *m/z* [M + H] calcd for $C_{25}H_{29}N_6O_2S$: 477.2067, found: 477.2032. Anal. Calcd for $C_{25}H_{33}Cl_5N_6O_2S(H_2O)_5$: C, 40.11; H, 6.19; N, 11.23; S, 4.28, found: C, 40.09; H, 5.84; N, 11.27; S, 4.56.

1,7-Bis(2-pyridylmethyl)-4-methyl-1,4,7-triazaheptane pentahydrochloride (**L5a·5HCl**). **L5** (1.02 g, 8.7 mmol) was reacted with 2-pyridinecarboxaldehyde (2.05 g, 1.91 mmol) according to the general procedure described above to give a pale yellow oil, which was then precipitated as its pentahydrochloride salt. Yield 2.6 g (99%); mp 188-191 °C; ^{1}H NMR (300 MHz, D_2O) δ 2.98 (s, 3H), 3.66 (s, 8H), 4.69 (s, 4H), 7.80 (ddd, *J* = 7.9, *J* = 5.5, *J* = 1.2, 2H), 7.87 (dt, *J* = 7.9, *J* = 1.2, 2H), 8.31 (td, *J* = 7.9, *J* = 1.7, 2H), 8.7 (ddd, *J* = 5.5, *J* = 1.7, *J* = 0.8, 2H); ^{13}C NMR (75 MHz, D_2O) δ 41.1 (CH_3), 42.5 (CH_2), 48.8 (CH_2), 52.6 (CH_2), 127.8 (CH), 127.9 (CH), 144.6 (CH), 146.2 (C), 146.7 (CH); HRMS (ESI+) *m/z* [M + H] calcd for $C_{17}H_{26}N_5$: 300.2183, found: 300.2212. Anal. Calcd for $C_{17}H_{30}Cl_5N_5(H_2O)_{1.5}$: C, 40.13; H, 6.54; N, 13.76, found: C, 40.02; H, 6.81; N, 13.35.

1,7-Bis(4-pyridylmethyl)-4-methyl-1,4,7-triazaheptane pentahydrochloride (**L5c·5HCl**). **L5** (0.57 g, 4.9 mmol) was reacted with 4-pyridinecarboxaldehyde (1.15 g, 10.7 mmol) according to the general procedure described above to give a pale yellow oil, which was then precipitated as its pentahydrochloride salt. Yield 1.41 g (97 %); mp 167-168 °C; ^{1}H NMR (300 MHz, D_2O) δ 2.80 (s, 3H), 3.44-3.49 (m, 4H), 3.60-3.69 (m, 4H), 4.65 (s, 4H), 8.17 (d, *J* = 6.8, 4H), 8.87 (d, *J* = 6.8, 4H); ^{13}C NMR (75 MHz, D_2O) δ 40.7 (CH_3), 43.5 (CH_2), 50.1 (CH_2), 52.7 (CH_2), 127.7 (CH), 142.5 (CH), 151.8 (C); HRMS (ESI+) *m/z* [M + H] calcd for $C_{17}H_{26}N_5$: 300.2183, found: 300.2194. Anal. Calcd for $C_{17}H_{30}Cl_5N_5(H_2O)_2$: C, 39.44; H, 6.62; N, 13.53, found: C, 39.36; H, 7.03; N, 13.56.

Synthesis of amides L1d and L2d. Methyl picolinate (4 equiv) was added dropwise under stirring to a solution of 4-*N*-substituted 1,4,7-triazaheptane compounds (**L1** or **L2**) (1 equiv) in MeOH (50 mL). The reaction mixture was heated to reflux under nitrogen atmosphere for 48 h. The reaction progress was monitored by TLC. After completion, the solvent was removed under reduced pressure and the crude was purified by column chromatography on silica gel. The resulting oil was dissolved in the minimum of dry CH_2Cl_2 and the amine was precipitated as its hydrochloride salt with 4 M HCl/dioxane solution (3 mL).

1,7-Bis(2-pyridinylcarbonyl)-4-(2-naphthylmethyl)-1,4,7-triazapentane trihydrochloride (**L1d·3HCl**). Following the general procedure described above, methyl picolinate (1.92 g, 14 mmol) was added under stirring to a solution of **L1** (1.55 g, 6.4 mmol). The residue was purified by column chromatography on silica gel (*n*-hexane/EtOAc 75:25) to give a light brown oil, which was then precipitated as its hydrochloride salt. Yield 0.92 g (32%); mp 217-221 °C; ^{1}H NMR (300 MHz, D_2O) δ 3.64 (t, *J* = 5.7, 4H), 3.78 (t, *J* = 5.7, 4H), 4.48 (s, 2H), 7.25-7.29 (m, 2H), 7.37 (dd, *J* = 8.5, *J* = 1.8, 1H), 7.42-7.45 (m, 1H), 7.50-7.53 (m, 2H), 7.78 (s, 1H), 7.89-7.91 (m, 4H), 8.30 (td, *J* = 7.9, *J* = 1.6, 2H), 8.53 (d, *J* = 5.4, 2H); ^{13}C NMR (75 MHz, D_2O) δ 36.2 (CH_2), 54.6 (CH_2), 59.4 (CH_2), 124.5 (CH), 126.5 (C), 127.5 (CH), 127.9 (CH), 128.0 (CH), 128.0 (CH), 128.3 (CH), 129.5 (CH), 129.7 (CH), 131.7 (CH), 132.6 (C), 133. 2 (C), 142.5 (C), 144.5 (CH), 145.7 (CH), 162.6 (CO); HRMS (ESI+) *m/z* [M + H] calcd for $C_{27}H_{28}N_5O_2$: 454.2238, found: 454.2250. Anal. Calcd. for $C_{27}H_{30}Cl_3N_5O_2(H_2O)_3$: C, 52.56; H, 5.88; N, 11.35, found: C, 52.55; H, 5.81; N, 11.30.

1,7-Bis(2-pyridinylcarbonyl)-4-(dansyl)-1,4,7-triazaheptane trihydrochloride (**L2d·3HCl**). Following the general procedure described above, methyl picolinate (0.67 g, 4.9 mmol) was added under stirring to a solution of **L2** (0.75 g, 2.2 mmol). The residue was purified by column chromatography on silica gel (CH_2Cl_2/MeOH 90:10) to give a pale yellow oil, which was then precipitated as its hydrochloride salt. Yield 0.71 g (58%); mp 186-189 °C; ^{1}H NMR (300 MHz, D_2O) δ 3.24 (s, 6H), 3.65 (t, *J* = 5.5, 4H), 3.83 (t, *J* = 5.5, 4H), 7.59 (t, *J* = 8.2, 1H), 7.68 (dd, *J* = 7.7, 1H), 7.77 (dd, *J* = 8.8, *J* = 7.5, 1H), 7.94 (ddd, *J* = 8, *J* = 5.5, *J* = 1.0, 2H), 7.99 (d, *J* = 8, 2H), 8.16 (d, *J* = 8.8, 1H), 8.27 (d, *J* = 7.4, 1H), 8.31 (d, *J* = 8.5, 1H), 8.36 (td, *J* = 8.0, *J* = 1.6, 2H), 8.64 (dd, *J* = 5.5, *J* = 1.7, 2H); ^{13}C NMR (75 MHz, D_2O) δ 37.1 (CH_2), 44.7 (CH_2), 47.0 (CH_3), 119.4 (CH), 124.2 (CH), 126.2 (CH), 126.9 (CH), 127.4 (CH), 128.4 (CH), 129.3 (CH), 132.3 (CH), 134.7 (C), 144.1 (C), 144.9 (CH), 145.12 (CH), 162. 4 (C), 177.3 (C); HRMS (ESI+) *m/z* [M + H] calcd for $C_{28}H_{31}N_6O_4S$: 547.2122, found: 547.2127. Anal. Calcd. for $C_{28}H_{33}Cl_3N_6O_4S(H_2O)_3$: C, 51.26; H, 5.07; N, 12.81; S, 4.89, found: C, 51.46; H, 5.26; N, 12.84; S, 5.01.

Electromotive force measurements. The potentiometric titrations were carried out in water at 298.1 ± 0.1 K using 0.15 mol dm^{-3} NaCl as the supporting electrolyte. NaCl was chosen as the inert electrolyte because of both the higher solubility of the compounds in this medium and the high content of this salt in extracellular fluids. The experimental procedure (burette, potentiometer, cell, stirrer, micro- computer, etc.) has been fully described elsewhere.[34] The acquisition of the EMF data was performed with the computer program PASAT.[35] The reference electrode was an Ag/AgCl electrode in saturated KCl solution. The glass electrode was calibrated as a hydrogen-ion concentration probe by titration of previously standardized amounts of HCl with CO_2-free NaOH solutions and the equivalent point determined by Gran's method,[26b,36] which gives the standard potential, E°', and the ionic product of water [pKw = 13.73(1)].[37] The computer program HYPERQUAD was used to calculate the protonation and stability constants.[26a] The pH range investigated (pH = −log[H+]) was 2.0–11.0 and the concentration of the metal ions and of the compound ranged from 1×10^{-3} to 5×10^{-3} M with 1:1 molar ratio. The different titration curves for each compound (at least two) were treated either as a single set or as separate curves without significant variations in the values of the stability constants. Finally, the sets of data were merged together and treated simultaneously to give the final stability constants.

Computational studies. The modelling of the Zn^{2+} complexes was performed using the density functional theory computational method as well as the Becke three-parameter Lee-Yang-Parr hybrid functional (B3LYP).[38] All the gas-phase optimizations were carried out using the Ahlrichs' basis set def2-SV(P)[39] for all atoms except for zinc for which we employed the MDF10 Stuttgart-Dresden effective core potential.[40] The influence of the dispersion was also taken into account by means of the Grimme's dispersion (*IOp(3/124=30)*) correction.[41] Vibrational frequencies were computed for each minimum energy structure and, for each one of them, it was also calculated and applied the zero-point correction. Calculations were performed without any symmetry constraints, and the effects of the solvent were included (water, ε = 78.39) self-consistently through the polarizable continuum model (PCM).[42] Computations were carried out using the program Gaussian09 C.01[43] gMolden[44] and PyMOL[45] were used for visual inspection and to create the molecular graphics.

Cell culture. Jurkat (Acute T-cell Leukemia, a gift from Prof. Joan Gil, IDIBELL, Barcelona), Jeko-1 (Non-Hodgkin Lymphoma, a gift from Beatriz Martínez, CNIO, Madrid), JVM-2, Granta-519 (Non-Hodgkin Lymphoma, a gift from Dr. Dolors Colomer, Hospital Clínic, Barcelona), Z-138, SP53, UPN-2 (Non-Hodgkin Lymphoma, a gift from Dr. Eva Ortega-Paino, Lund University, Lund), were maintained in RPMI-1640 with L-Glutamine and HEPES (Biological Industries Ltd., Kibbutz Beit Haemek, Israel). LN229, U251, U373 and U87MG (Glioma, a gift from Dr. Joan Seoane,

Institut de Recerca Vall d'Hebron, Barcelona), SKMG-3 (Glioma, a gift from Dr.Hans Skovgaard, Rigshospitalet, Oslo), PC-3 (Prostate Cancer, a gift from Prof. Anne J. Ridley, King's College, London), SW480 and SW620 (Colorectal cancer, a gift from Prof. Eric Lam, Imperial College, London), MCF-7 (Breast Cancer, a gift from Prof. Eric Lam, Imperial College, London), cells were maintained in DMEM High Glucose (4.5 g/l) with L-glutamine (Invitrogen, Carlsbad, CA). Fibroblast cells derived from individuals were kindly provided by the group of Molecular therapies of the University of Valencia. All cells were grown in a humidified incubator at 37 ºC with 5% CO_2. RPMI and DMEM were supplemented with 10% heat inactivated fetal bovine serum and 100 units/mL penicillin/streptomycin (Sigma-Aldrich, St Louis, MO). All cell lines were subconfluently grown and passaged, routinely tested for mycoplasma contamination and subjected to frequent morphological tests and growth curve analysis as quality-control assessments. All cell lines were treated at a prophylactic concentration of 5 μg/ml Plasmocin™ (InvivoGen, San Diego, CA).

Cell viability analysis. The number of viable cells in culture was determined based on quantification of ATP, which signals the presence of metabolically-active cells, using the Cell Titer-Glo luminescent assay kit (Promega, Madison, WI). Following the manufacturer's instructions, the cells were plated in 96-well plates, treated 24 h later with the compounds for the indicated times and concentrations, followed by addition of Cell Titer-Glo reagent. Luminescence was detected using a multi-well Synergy Mx scanning spectrophotometer (Biotek, Winooski, VT).

The effect of metal ions on the cell viability was assessed using the colorimetric MTT ([3-(4,5- dimethylthiazol-2-yl)-2,5-diphenyltetrazolium bromide]) method.[45] Briefly, LN229 and PC3 cells were plated in 96-well plates and treated 24 h later with **L1a** (10 μM) and **L5a** (10 μM) in presence or absence of metal ions Zn^{2+}, Cu^{2+}, Fe^{2+} or Fe^{3+} (15 μM) for 48 h. After incubation, the supernatant was discarded and 100 μL medium and 10 μL MTT (12 mM) solution were added into the wells and incubated for another 4 h. The media was removed and the cells solubilized using 100 μL DMSO. Optical density (OD) absorbance readings were determined using a Thermo Multiskan EX plate reader (Thermo scientific) at 540 nm. The values obtained for **L1a** or **L5a**-treatments were reproducible.

Cell cycle analysis. Cell cycle analysis was performed using propidium iodide staining. Briefly, cells were washed in phosphate-buffered saline (PBS) and fixed in 70% ethanol (Sigma-Aldrich, St Louis, MO). Fixed cells were then washed twice in PBS and stained with 50 μg/ml propidium iodide (Sigma-Aldrich, St Louis, MO) in the presence of 50 μg/ml RNase A (Sigma-Aldrich, St Louis, MO), then analyzed by flow cytometry using a FACScan (Coulter Epics XL-MSL, Beckman Coulter, Fullerton, CA). Percent distributions the DNA content of the samples in G0/G1, S and G2/M phases of the cell cycle were analyzed with Flowing Software version 2.5.1 (Perttu Terho, Turku Centre for Biotechnology, Finland; www.flowingsoftware.com).

Annexin V-FITC / propidium iodide flow cytometric analysis. Analysis of phosphatidyl serine externalization in apoptotic cells was determined by an ApoTarget Annexin-V-FITC Apoptosis kit (Invitrogen, Carlsbad, CA), according to the manufacturer's instructions. 2 x 10^5 cells were seeded in 6-well plates and treated as indicated. Cells were then collected and suspended in 100 μl of Annexin V-binding buffer. 5 μL of Annexin-V-FITC and 10μL of propidium iodide were added and incubated 15 min at room temperature in the dark. Flow cytometry analysis was carried out using a FACScan (Coulter Epics XL-MSL, Beckman Coulter, Fullerton, CA) and winMDI software.

Caspase activity analysis. Enzymatic activity of caspases was determined by measurement of caspases-3 and 7 activity by means of the luminometric Caspase-Glo 3/7 assay (Promega, Madison, WI) according to the manufacturer's protocol using a Synergy HT multi-detection microplate reader (Bio-Tek, Winooski, VT).

γ-H2A.X quantification. DNA damage was assessed monitoring the intensity of γ-H2A.X fluorescence using flow cytometry. Briefly, trypsinized cells were collected by centrifugation, washed in PBS and fixed in 3.7% formaldehyde (Sigma-Aldrich, St Louis, MO) for 15 min on ice. Cells were then permeabilized with 0.2% v/v Triton-X (Sigma-Aldrich, St Louis, MO) for 10 min, and incubated with 1:400 rabbit anti-p-(S139)-H2A.X antibody (Cell Signaling Technology, Beverly, MA) for 30 min on ice, washed in Triton-X 0.1% in PBS and incubated with 1:400 anti-rabbit Alexa 555-conjugated antibody (Jackson Immuno Research, West Grove, PA) for 20 min on ice and washed. Flow cytometry analysis was carried out using a FACScan (Coulter Epics XL-MSL, Beckman Coulter, Fullerton, CA) and Flowing software.

Clonogenic assays. Cells were seeded in 12-well plates. 24 h later, cells were treated for 4h with 10 μM **L1a** and **L5a** or vehicle alone as a control. Cells were then washed with PBS, trypsinized and plated at low density (3000 cells/60-mm plate). Cells were allowed to divide and form colonies for 7–10 days. The colonies were fixed and stained with 0.5% (w/v) crystal violet (Sigma-Aldrich, St. Louis, MO) in 70% ethanol and the number of colonies counted. All experiments were performed in triplicate.

Senescence assays. Cytochemical senescence detection was performed with the Senescence Cells Histochemical Staining Kit (CS0030, Sigma-Aldrich, St. Louis, MO) according to the manufacturer's instructions. Briefly, LN229 and PC3 cells were cultured in 6-well plates at 12 x 10^4 cells/well and treated with 10 μM of selected compounds **L1a** and **L5a** for 24 h. The cultured medium was removed and the cells were then washed with PBS and fixed with 2% formaldehyde, 0.2% glutaraldehyde solution (1 mL) for 10 min at room temperature. The cells were washed again and stained in 1 mL 1x staining solution containing 1 mg/mL 5-bromo-4-chloro-3-indolyl-β-*D*-galactopyranoside (X-gal) and 1x staining supplements at 37 °C for 24 h without CO_2 circulation. Cells were then overlaid with 70% glycerol and observed under microscope for development of blue color. Blue-stained cells were counted in at least 10 fields at 10x magnification and the number of stained cells was expressed as the percentage of positive cells relative to total cell number.

Mitochondrial membrane potential (Ψ_m) analysis. The MMP was monitored using the dual-emission mitochondrial dye JC-1, 5,5,6,6-tetrachloro-1,1,3,3-tetraethylbenzimidazole carbocyanide iodide (MitoProbe™ JC-1 assay Kit, Molecular Probes) according to the manufacturer's instructions. At high mitochondrial membrane potentials, JC-1 accumulates in the mitochondria and forms J-aggregates that show a red fluorescence emission at 590 nm, but with de-energized or depolarized mitochondria, less dye enters to mitochondria resulting in monomers that show green fluorescence emission at 530 nm. Briefly, LN229 cells were seeded in 6-well plates at a density of 5 x 10^5 cells/mL and allowed to adhere overnight. Culture medium was replaced with fresh medium containing polyamines **L1a** (10 μM) and **L5a** (10 μM). After incubation for 24 h, cells were trypsinized, washed with phosphate-buffered saline (PBS) and incubated with JC-1 dye (2 μM) at 37 ºC for 30 min. Then, cells were pelleted by centrifugation at 1500 rpm for 5 min at room temperature, washed by adding PBS and analyzed by flow cytometry on a flow cytometer Coulter EPICS-XL (Beckman Coulter, Fullerton, CA). In each experiment, at least 10.000 events were analyzed. JC-1 monomer fluorescence signals were detected on the filter 1 (FL1) detector (green fluorescence, 530 nm) and JC-1 aggregate fluorescence signals on the FL3 detector (red fluorescence, 590 nm). Mean fluorescence intensity values for FL1 and FL3 are expressed as FL3/FL1 ratio.

Intracellular zinc measurements by *Zinquin* Fluorescence assay. *Zinquin* ester (ethyl (2-methyl-8-p-toluenesulfonamido-6-quinolyloxy)acetate, ENZO) was used to quantify the level of free labile intracellular Zn(II) upon treatment with the selected compounds by spectrofluorometry using a standard method adopted from Zalewski *et al*.[22b] After treatment with polyamines **L1a** and **L5a** for 12h, LN229 and PC3 cells were trypsinized and harvested by centrifugation at 1000 rpm for 5 min. Cell viability was assessed by Trypan Blue stain and then 6x10^6 cells were resuspended in PBS (1 mL) and incubated in the dark with *Zinquin* (25 μM) at 37 °C for 30 min. Cell suspensions were transferred to an ultraviolet-grade cuvette and the fluorescence count was measured at 370 nm excitation and 475 nm (slit width 3 nm) emission wavelengths and scans of the fluorescence emission between 400 and 600 nm. All spectrofluorometric experiments were performed with a spectrofluorometer (PTI) equipped with a lamp power supply LPS-220B, MD-5020 and an 814 Photomultiplier Detection System.

Multiphoton confocal microscopy. Multiphoton confocal microscopy was assessed using an Olympus FV1000MPE microscope. Briefly, LN229 cells were cultured in 65 mm plates at 1x10^4 cells/plate. After incubation for 24 h, cells were treated with 10 μM and 20 μM of selected compounds for 6h. The cultured medium was removed and washed with PBS, leaving finally 2 mL of PBS per plate. The images were acquired exciting at 700 nm.

Statistical analysis. All of the presented data as means ± SD were obtained based on three independent experiments and were analyzed with GraphPad Prism software (GraphPad Software Inc. La Jolla, CA). Significant differences between control and treated groups were assessed using Student's *t*-test. Analysis of variance (ANOVA) followed by Turkey's post hoc analysis were used to determine the statistical significance among treatments conditions and cell lines. Statistically significant differences are indicated by ****p<0.0001, ***p<0.001, **p<0.01 and *p<0.05.

ASSOCIATED CONTENT

Supporting Information. ^{1}H, ^{13}C, COSY, HSQC NMR collection spectra, **L1a** and **L5a** HPLC purity spectra, cell viability information, stepwise basicity constants, distribution diagrams, stability constants and quantum mechanical studies for selected **L1**-**L5** Zn^{2+} complexes (PDF)
Molecular formula strings and some data (CSV)
This material is available free of charge via the Internet at http://pubs.acs.org.

AUTHOR INFORMATION

Corresponding Author

*eugenia@uchceu.es
*cristina.galiana@uv.es
*priam.villalonga@uib.es
*Enrique.Garcia-Es@uv.es

ORCID

Silvia Fernández de Mattos: 0000-0003-4144-3687
Cristina Galiana-Roselló: 0000-0003-1365-1323
Jorge González García: 0000-0001-8994-1779
M. Eugenia González-Rosende: 0000-0002-3566-294X
José M. Llinares Berenguer: 0000-0003-3763-4317
Álvaro Martínez-Camarena: 0000-0001-9910-6961
Enrique García-España: 0000-0002-4601-6505
Priam Villalonga: 0000-0001-7037-1550
Ruth Villalonga-Planells: 0000-0002-5930-8435

Notes

The authors declare no competing financial interest.

ACKNOWLEDGMENT

This work was supported by the Spanish MINECO and FEDER funds from the E.U. (Consolider-Ingenio, Project CSD2010-000652010 and CTQ2013-48917-C3-1-P) and Generalitat Valenciana (PROMETEO II 2015/002). C.G-R. and A. M.–C. thank the Ministry of Education of Spain for a FPU Grant. We are grateful to Joan Seoane (Institut de Recerca Hospital Vall d'Hebron, Barcelona), Hans Skovgaard (Rigshospitalet, Oslo), Dolors Colomer (Hospital Clínic, Barcelona), Eric Lam (Imperial College, London), Anne J. Ridley (University of Bristol), Eva Ortega-Paino (Lund University, Lund) and Beatriz Martínez (CNIO, Madrid) for cell lines.

ABBREVIATIONS

NMEs, New Molecular Entities; NPs, Natural Products; DIEN, 1,4,7-triazaheptane; MMP, Mitochondrial Membrane Potential; DNA-DSBs, DNA Double Strand Breaks; DDR, DNA Damage Response, QM, quantum mechanical; SAR, Structure-Activity Relationship.

REFERENCES

(1) Ferlay, J.; Soerjomataram, I.; Dikshit, R.; Eser, S.; Mathers, C.; Rebelo, M.; Parkin, D. M.; Forman, D.; Bray, F., Cancer Incidence and Mortality Worldwide: Sources, Methods and Major Patterns in GLOBOCAN 2012. *Int. J. Cancer* **2015,** *136* (5), E359-386.

(2) World Health Organization (WHO). Cancer. https://www.who.int/news-room/fact-sheets/detail/cancer (accessed Jun 14, 2019).

(3) Kinch, M. S., An Analysis of FDA-approved Drugs for Oncology. *Drug Discovery Today* **2014,** *19* (12), 1831-1835.

(4) (a) Newman, D. J.; Cragg, G. M., Natural Products as Sources of New Drugs from 1981 to 2014. *J. Nat. Prod.* **2016,** *79* (3), 629-661; (b) Harvey, A. L., Natural Products in Drug Discovery. *Drug Discovery Today* **2008,** *13* (19), 894-901; (c) Gordaliza, M., Natural Products as Leads to Anticancer drugs. *Clin. Transl. Oncol.* **2007,** *9* (12), 767-776.

(5) (a) Minois, N., Molecular Basis of the 'Anti-aging' Effect of Spermidine and other Natural Polyamines - a mini-review. *Gerontology* **2014,** *60* (4), 319-326; (b) Muth, A.; Kamel, J.; Kaur, N.; Shicora, A. C.; Ayene, I. S.; Gilmour, S. K.; Phanstiel, O., Development of Polyamine Transport Ligands with Improved Metabolic Stability and Selectivity Against Specific Human Cancers. *J. Med. Chem.* **2013,** *56* (14), 5819-5828; (c) Nowotarski, S. L.; Woster, P. M.; Casero, R. A., Jr., Polyamines and Cancer: Implications for Chemotherapy and Chemoprevention. *Expert. Rev. Mol. Med.* **2013,** *15*, e3; (d) Gerner, E. W.; Meyskens, F. L., Jr., Polyamines and Cancer: Old Molecules, New Understanding. *Nat. Rev. Cancer* **2004,** *4* (10), 781-792.

(6) Bolognesi, M. L.; Minarini, A.; Budriesi, R.; Cacciaguerra, S.; Chiarini, A.; Spampinato, S.; Tumiatti, V.; Melchiorre, C., Universal Template Approach to Drug Design: Polyamines as Selective Muscarinic Receptor Antagonists. *J. Med. Chem.* **1998,** *41* (21), 4150-4160. (b) Casero, R.A.; Stewart, T.; Pegg, A.E., Polyamine Metabolism and Cancer: Treatments, Challenges and Opportunities. *Nat. Rev. Cancer* **2018,** *18*, 681-695. (c) Bae, D.H.; Lane, D.J.R.; Jansson, P.J.; Richardson, D.R., The Old and New Biochemistry of Polyamines. *Biochim. Biophys. Acta Gen. Subj.* **2018**, *1862*, 2053–2068.

(7) (a) Dai, F.; Li, Q.; Wang, Y.; Ge, C.; Feng, C.; Xie, S.; He, H.; Xu, X.; Wang, C., Design, Synthesis, and Biological Evaluation of Mitochondria-Targeted Flavone-Naphthalimide-Polyamine Conjugates with Antimetastatic Activity. *J. Med. Chem.* **2017,** *60* (5), 2071-2083; (b) Milelli, A.; Marchetti, C.; Greco, M. L.; Moraca, F.; Costa, G.; Turrini, E.; Catanzaro, E.; Betari, N.; Calcabrini, C.; Sissi, C.; Alcaro, S.; Fimognari, C.; Tumiatti, V.; Minarini, A., Naphthalene Diimide-Polyamine Hybrids as Antiproliferative Agents: Focus on the Architecture of the Polyamine Chains. *Eur. J. Med. Chem.* **2017,** *128*, 107-122; (c) Moosa, B. A.; Sagar, S.; Li, S.; Esau, L.; Kaur, M.; Khashab, N. M., Synthesis and Anticancer Evaluation of Spermatinamine Analogues. *Bioorg. Med. Chem. Lett.* **2016,** *26* (6), 1629-1632; (d) Weisell, J.; Hyvonen, M. T.; Alhonen, L.; Vepsalainen, J.; Keinanen, T. A.; Khomutov, A. R., Charge Deficient Analogues of the Natural Polyamines. *Curr. Pharm. Des.* **2014,** *20* (2), 262-277; (e) Pasini, A.; Caldarera, C. M.; Giordano, E., Chromatin Remodeling by Polyamines and Polyamine Analogs. *Amino Acids* **2014,** *46* (3), 595-603; (f) Minarini, A.; Zini, M.; Milelli, A.; Tumiatti, V.; Marchetti, C.; Nicolini, B.; Falconi, M.; Farruggia, G.; Cappadone, C.; Stefanelli, C., Synthetic Polyamines Activating Autophagy: Effects on Cancer Cell Death. *Eur. J. Med. Chem.* **2013,** *67*, 359-366; (g) *Polyamine Drug Discovery*; Woster, P., Casero R., Eds.; Drug Discovery Series; Royal Society of Chemistry: RSC Publishing, 2012; (h) Minarini, A.; Milelli, A.; Tumiatti, V.; Rosini, M.; Bolognesi, M. L.; Melchiorre, C., Synthetic Polyamines: An Overview of their Multiple Biological Activities. *Amino Acids* **2010,** *38* (2), 383-392; (i) Casero, R. A.; Woster, P. M., Recent Advances in the Development of Polyamine Analogues as Antitumor Agents. *J. Med. Chem.* **2009,** *52* (15), 4551-4573.

(8) (a) Merlot, A. M.; Kalinowski, D. S.; Kovacevic, Z.; Jansson, P. J.; Sahni, S.; Huang, M. L.; Lane, D. J. R.; Lok, H.; Richardson, D. R., Exploiting Cancer Metal Metabolism using Anti-Cancer Metal-Binding Agents. *Curr. Med. Chem.* **2019,** *26* (2), 302-322; (b) Kang, C. S.; Ren, S.; Sun, X.; Chong, H. S., Theranostic Polyaminocarboxylate-Cyanine-Transferrin Conjugate for Anticancer Therapy and Near-Infrared Optical Imaging. *ChemMedChem* **2016,** *11* (19), 2188-2193; (c) Merlot, A. M.; Kalinowski, D. S.; Richardson, D. R., Novel Chelators for Cancer Treatment: Where are we now? *Antioxid. Redox Signaling* **2013,** *18* (8), 973-1006; (d) Rafique, S.; Idrees, M.; Nasim, A.; Akbar, H.; Athar, A., Transition Metal Complexes as Potential Therapeutic Agent. *Biotechnol. Mol. Biol. Rev.* **2010,** *5* (2), 38-45.

(9) (a) Yu, Y.; Gutierrez, E.; Kovacevic, Z.; Saletta, F.; Obeidy, P.; Suryo Rahmanto, Y.; Richardson, D. R., Iron Chelators for the Treatment of Cancer. *Curr. Med. Chem.* **2012,** *19* (17), 2689-2702; (b) Fatfat, M.; Merhi, R. A.; Rahal, O.; Stoyanovsky, D. A.; Zaki, A.; Haidar, H.; Kagan, V. E.; Gali-Muhtasib, H.; Machaca, K., Copper Chelation Selectively Kills Colon Cancer Cells Through Redox Cycling and Generation of Reactive Oxygen Species. *BMC Cancer* **2014,** *14* (1), 1-12; (c) Santini, C.; Pellei, M.; Gandin, V.; Porchia, M.; Tisato, F.; Marzano, C., Advances in Copper Complexes as Anticancer Agents. *Chem. Rev.* **2014,** *114* (1), 815-862; (d) Hyvonen, M. T.; Ucal, S.; Pasanen, M.; Peraniemi, S.; Weisell, J.; Khomutov, M.; Khomutov, A. R.; Vepsalainen, J.; Alhonen, L.; Keinanen, T. A., Triethylenetetramine Modulates Polyamine and Energy Metabolism and Inhibits Cancer Cell Proliferation. *Biochem. J.* **2016,** *473* (10), 1433-1441.

(10) Franklin, R. B.; Costello, L. C., The Important Role of the Apoptotic Effects of Zinc in the Development of Cancers. *J. Cell. Biochem.* **2009,** *106* (5), 750-757.

(11) (a) Hashemi, M.; Ghavami, S.; Eshraghi, M.; Booy, E. P.; Los, M., Cytotoxic effects of intra and extracellular zinc chelation on human breast cancer cells. *Eur. J. Pharmacol.* **2007,** *557* (1), 9-19; (b) Hyun, H. J.; Sohn, J. H.; Ha, D. W.; Ahn, Y. H.; Koh, J. Y.; Yoon, Y. H., Depletion of Intracellular Zinc and Copper with TPEN Results in Apoptosis of Cultured Human Retinal Pigment Epithelial Cells. *Invest. Ophthalmol. Visual Sci.* **2001,** *42* (2), 460-465. (c) Nakatani, T.; Tawaramoto, M.; Kennedy, D.O.; Kojima, A.; Matsui-Yuasa, I., Apoptosis Induced by Chelation of Intracellular Zinc is Associated with Depletion of Cellular Reduced Glutathione Level in Rat Hepatocytes. *Chem-Biol. Interact.* **2000**, *125* (3), 151-163.

(12) (a) Silva, T. M.; Fiuza, S. M.; Marques, M. P.; Persson, L.; Oredsson, S., Increased Breast Cancer Cell Toxicity by Palladination of the Polyamine Analogue N^1,N^{11}-bis(ethyl)norspermine. *Amino Acids* **2014,** *46* (2), 339-352; (b) Corcé, V.; Renaud, S.; Cannie, I.; Julienne, K.; Gouin, S. G.; Loréal, O.; Gaboriau, F.; Deniaud, D., Synthesis and Biological Properties of Quilamines II, New Iron Chelators with Antiproliferative Activities. *Bioconjugate Chem.* **2014,** *25* (2), 320-334; (c) Åstrand, O. A. H.; Aziz, G.; Ali, S. F.; Paulsen, R. E.; Hansen, T. V.; Rongved, P., Synthesis and Initial in vitro Biological Evaluation of Two New Zinc-Chelating Compounds: Comparison with TPEN and PAC-1. *Bioorg. Med. Chem.* **2013,** *21* (17), 5175-5181; (d) Rojas-Valencia, L.; Velez-Pardo, C.; Jimenez-Del-Rio, M., Metal Chelator TPEN Selectively Induces Apoptosis in K562 Cells through Reactive Oxygen Species Signaling Mechanism: Implications for Chronic Myeloid Leukemia. *BioMetals* **2017,** *30* (3), 405-421.

(13) (a) Makhov, P.; Golovine, K.; Uzzo, R. G.; Rothman, J.; Crispen, P. L.; Shaw, T.; Scoll, B. J.; Kolenko, V. M., Zinc Chelation Induces Rapid Depletion of the X-linked Inhibitor of Apoptosis and Sensitizes Prostate Cancer Cells to TRAIL-Mediated Apoptosis. *Cell Death Differ.* **2008,** *15* (11), 1745–1751; (b) Zhu, B.; Wang, J.; Zhou, F.; Liu, Y.; Lai, Y.; Wang, J.; Chen, X.; Chen, D.; Luo, L.; Hua, Z. C., Zinc Depletion by TPEN Induces Apoptosis in Human Acute Promyelocytic NB4 Cells. *Cell. Physiol. Biochem.* **2017,** *42* (5), 1822-1836.

(14) Aceves-Luquero, C.; Galiana-Roselló, C.; Ramis, G.; Villalonga-Planells, R.; García-España, E.; Fernández de Mattos, S.; Pélaez, R.; Llinares, J. M.; González-Rosende, M. E.; Villalonga, P., *N*-(2-methyl-indol-1H-5-yl)-1-naphthalenesulfonamide: A Novel Reversible Antimitotic Agent Inhibiting Cancer Cell Motility. *Biochem. Pharmacol.* **2016,** *115*, 28-42.

(15) Aucejo, R.; Alarcón, J.; García-España, E.; Llinares, J. M.; Marchin, K. L.; Soriano, C.; Lodeiro, C.; Bernardo, M. A.; Pina, F.; Pina, J.; de Melo, J., A New Zn^{II} Tweezer Pyridine-Naphthalene System - An off-on-off System Working in a Biological pH Window. *Eur. J. Inorg. Chem.* **2005,** 4301-4308.

(16) Itahana, K.; Campisi, J.; Dimri, G. P., Methods to Detect Biomarkers of Cellular Senescence: The Senescence-Associated Beta-Galactosidase Assay. *Methods Mol. Biol.* **2007,** *371*, 21-31.

(17) Kroemer, G.; Zamzami, N.; Susin, S. A., Mitochondrial Control of Apoptosis. *Immunol. Today* **1997,** *18* (1), 44-51.

(18) Perelman, A.; Wachtel, C.; Cohen, M.; Haupt, S.; Shapiro, H.; Tzur, A., JC-1: Alternative Excitation Wavelengths Facilitate Mitochondrial Membrane Potential Cytometry. *Cell Death Dis.* **2012,** *3*, e430.

(19) N'Soukpoe-Kossi, C. N.; Ouameur, A. A.; Thomas, T.; Shirahata, A.; Thomas, T. J.; Tajmir-Riahi, H. A., DNA Interaction with Antitumor Polyamine Analogues: A Comparison with Biogenic Polyamines. *Biomacromolecules* **2008,** *9* (10), 2712-2718.

(20) (a) Suzuki, I.; Shigenaga, A.; Nemoto, H.; Shibuya, M., Synthesis and DNA Damaging Ability of Enediyne–Polyamine Conjugates. *Tetrahedron Lett.* **2004,** *45* (9), 1955-1959; (b) Xu, H.; Chaturvedi, R.; Cheng, Y.; Bussiere, F. I.; Asim, M.; Yao, M. D.; Potosky, D.; Meltzer, S. J.; Rhee, J. G.; Kim, S. S.; Moss, S. F.; Hacker, A.; Wang, Y.; Casero, R. A., Jr.; Wilson, K. T., Spermine Oxidation Induced by *Helicobacter pylori* Results in Apoptosis and DNA damage: Implications for Gastric Carcinogenesis. *Cancer Res.* **2004,** *64* (23), 8521-8525.

(21) Lukas, J.; Lukas, C.; Bartek, J., More than Just a Focus: The Chromatin Response to DNA Damage and its Role in Genome Integrity Maintenance. *Nat. Cell Biol.* **2011,** *13* (10), 1161-1169.

(22) (a) Zalewski, P. D.; Forbes, I. J.; Betts, W. H., Correlation of Apoptosis with Change in Intracellular Labile Zn(II) using Zinquin [(2-methyl-8-*p*-toluenesulphonamido-6-quinolyloxy) acetic acid], a New Specific Fluorescent Probe for Zn(II). *Biochem. J.* **1993,** *296* (Pt 2), 403–408; (b) Zalewski, P.; Truong-Tran, A.; Lincoln, S.; Ward, D.; Shankar, A.; Coyle, P.; Jayaram, L.; Copley, A.; Grosser, D.; Murgia, C.; Lang, C.; Ruffin, R., Use of a Zinc Fluorophore to Measure Labile Pools of Zinc in Body Fluids and Cell-Conditioned Media. *Biotechniques* **2006,** *40* (4), 509-520.

(23) Huesca, M.; Lock, L. S.; Khine, A. A.; Viau, S.; Peralta, R.; Cukier, I. H.; Jin, H.; Al-Qawasmeh, R. A.; Lee, Y.; Wright, J.; Young, A., A novel Small Molecule with Potent Anticancer Activity Inhibits Cell Growth by Modulating Intracellular Labile Zinc Homeostasis. *Mol. Cancer Ther.* **2009,** *8* (9), 2586-2596.

(24) Donadelli, M.; Dalla Pozza, E.; Costanzo, C.; Scupoli, M. T.; Scarpa, A.; Palmieri, M., Zinc Depletion Efficiently Inhibits Pancreatic Cancer Cell Growth by Increasing the Ratio of Antiproliferative/Proliferative Genes. *J. Cell Biochem.* **2008,** *104* (1), 202-212.

(25) (a) Parola, A. J.; Lima, J. C.; Pina, F.; Pina, J.; Melo, J. S. d.; Soriano, C.; García-España, E.; Aucejo, R.; Alarcón, J., Synthesis and Photophysical Properties of Dansyl-Based Polyamine Ligands and their Zn(II) Complexes. *Inorg. Chim. Acta* **2007,** *360* (3), 1200-1208; (b) Rodriguez, L.; Lima, J. C.; Parola, A. J.; Pina, F.; Meitz, R.; Aucejo, R.; García-España, E.; Llinares, J. M.; Soriano, C.; Alarcón, J., Anion Detection by Fluorescent Zn(II) Complexes of Functionalized Polyamine Ligands. *Inorg. Chem.* **2008,** *47* (14), 6173-6183.

(26) (a) Gans, P.; Sabatini, A.; Vacca, A., Investigation of Equilibria in Solution. Determination of Equilibrium Constants with the HYPERQUAD suite of programs. *Talanta* **1996,** *43* (10), 1739-1753; (b) Rossotti, F. J. C.; Rossotti, H., Potentiometric Titrations using Gran Plots: A textbook Omission. *J. Chem. Educ.* **1965,** *42* (7), 375-378.

(27) (a) Chmielewski, M. J.; Jurczak, J., Anion Recognition by Neutral Macrocyclic Amides. *Chem. Eur. J.* **2005,** *11* (20), 6080-6094; (b) Hossain, M. A.; Kang, S. O.; Powell, D.; Bowman-James, K., Anion Receptors: A New Class of Amide/Quaternized Amine Macrocycles and the Chelate Effect. *Inorg. Chem.* **2003**, *42* (5), 1397-1399.

(28) Manallack, D. T.; Prankerd, R. J.; Yuriev, E.; Oprea, T. I.; Chalmers, D. K., The Significance of Acid/Base Properties in Drug discovery. *Chem. Soc. Rev.* **2013,** *42* (2), 485-496.

(29) (a) Zvimba, J. N.; Jackson, G. E., Solution Equilibria of Copper(II) Complexation with *N*,*N*'-(2,2'-azanediylbis(ethane-2,1-diyl))dipicolinamide: A Bio-Distribution and Dermal Absorption Study. *J. Inorg. Biochem.* **2007,** *101* (8), 1120-1128; (b) Rowland, J. M.; Thornton, M. L.; Olmstead, M. M.; Mascharak, P. K., Structure Variation Due to Ligand Flexibility: Syntheses and Structures of the Copper(II) Complexes [Cu(APPy)] and $[Cu_2(AEPy)_2]$ Where $APPyH_2$ = Bis[3-(2-pyridinecarboxamido)propyl]-methylamine and $AEPyH_2$ = Bis[3-(2-pyridine-carboxamido)ethyl]methylamine. *Inorg. Chem.y* **2001,** *40* (5), 1069-1073; (c) Hubert, S.; Mohamadou, A.; Gérard, C.; Marrot, J., Equilibrium and Structural Studies of Copper and Nickel Complexes with a Pentadentate Ligand Providing Amide, Amine and Pyridyl Nitrogen Donors. Crystal Structure of the Dinuclear Nickel(II) Complex. *Inorg. Chim. Acta* **2007,** *360* (5), 1702-1710.

(30) Torti, S. V.; Ma, R.; Venditto, V. J.; Torti, F. M.; Planalp, R. P.; Brechbiel, M. W., Preliminary Evaluation of the Cytotoxicity of a Series of Tris-2-aminoethylamine (Tren) Based Hexadentate Heterocyclic Donor Agents. *Bioorg. Med. Chem.* **2005,** *13* (21), 5961-5967.

(31) (a) Kurishita, Y.; Kohira, T.; Ojida, A.; Hamachi, I., Organelle-Localizable Fluorescent Chemosensors for Site-Specific Multicolor Imaging of Nucleoside Polyphosphate Dynamics in Living Cells. *J. Am. Chem. Soc.* **2012,** *134* (45), 18779-18789; (b) Pont, I.; Galiana-Roselló, C.; Lopera, A.; González-García, J.; García-España, E., Recognition, Transformation, Detection of Nucleotides and Aqueous Nucleotide-Based Materials. In *Supramolecular Chemistry in Water*, Kubik, S., Eds.; Wiley-VCH Verlag GmbH & Co., 2019; pp 115-160.

(32) SwissADME Home Page. http://www.swissadme.ch/index.php (accessed Jun 18, 2019).

(33) Onopchenko, A.; Harrison, J. J.; Chan, C. Y., The Reaction of Phthalic Anhydride with Diethylenetriamine and Triethylenetetramine. A Literature Correction. *Bull. Chem. Soc. Jpn.* **1998,** *71* (3), 717-721.

(34) García-España, E.; Ballester, M.-J.; Lloret, F.; Moratal, J. M.; Faus, J.; Bianchi, A., Low-Spin Six-Co-ordinate Cobalt(II) Complexes. A Solution Study of Tris(violurato)cobaltate(II) Ions. *J. Chem. Soc., Dalton Trans.* **1988,** 101-104.

(35) M. Fontanelli, M. M. Program for the Automatic Control of Microburette and the Acquisition of the Electromotive Force Readings. *Proceedings of the I Spanish-Italian Congress on Thermodynamics of the Metal Complexes*, Castellón, Spain, 1990.

(36) Gran, G., Determination of the Equivalence Point in Potentiometric Titrations. Part II. *Analyst* **1952,** *77* (920), 661-671.

(37) Avdeef, A.; Box, K. J.; Comer, J. E.; Gilges, M.; Hadley, M.; Hibbert, C.; Patterson, W.; Tam, K. Y., pH-metric logP 11. pKa Determination of Water-Insoluble Drugs in Organic Solvent-Water Mixtures. *J. Pharm. Biomed. Anal.* **1999,** *20* (4), 631-641.

(38) (a) Perdew, J. P., Density-Functional Approximation for the Correlation Energy of the Inhomogeneous Electron Gas. *Phys. Rev. B: Condens. Matter Mater. Phys.* **1986,** *33* (12), 8822-8824; (b) Becke, A. D., Density-Functional Exchange-Energy Approximation with Correct Asymptotic Behavior. *Phys. Rev. A* **1988,** *38* (6), 3098-3100; (c) Lee, C.; Yang, W.; Parr, R. G., Development of the Colle-Salvetti Correlation-Energy Formula into a Functional of the Electron Density. *Phys. Rev. B: Condens. Matter Mater. Phys.* **1988,** *37* (2), 785-789.

(39) Weigend, F.; Ahlrichs, R., Balanced Basis Sets of Split Valence, Triple Zeta Valence and Quadruple Zeta Valence Quality for H to Rn: Design and Assessment of Accuracy. *Phys. Chem. Chem. Phys.* **2005,** *7* (18), 3297-3305.

(40) Andrae, D.; Häußermann, U.; Dolg, M.; Stoll, H.; Preuß, H., Energy-Adjusted ab initio Pseudopotentials for the Second and Third Row Transition Elements. *Theor. Chim. acta* **1990,** *77* (2), 123-141.

(41) Grimme, S., Antony, J., Ehrlich, S., Krieg, H., A Consistent and Accurate ab initio Parametrization of Density Functional Dispersion Correction (DFT-D) for the 94 Elements H-Pu. *J. Chem. Phys.* **2010,** *132* (15), 154104.

(42) (a) Tomasi, J.; Mennucci, B.; Cammi, R. Quantum Mechanical Continuum Solvation Models. *Chem. Rev*. **2005**, *105*, 2999–3093;

(b) Cossi, M.; Scalmani, G.; Rega, N.; Barone, V. New Developments in the Polarizable Continuum Model for Quantum Mechanical and Classical Calculations on Molecules in Solution. *J. Chem. Phys.* **2002**, *117*, 43–54.

(43) *Gaussian 09*, Revision C.01; Frisch, M. J.; Trucks, G. W.; Schlegel, H. B.; Scuseria, G. E.; Robb, M. A.; Cheeseman, J. R.; Scalmani, G.; Barone, V.; Mennucci, B.; Petersson, G. A.; Nakatsuji, H.; Caricato, M.; Li, X.; Hratchian, H. P.; Izmaylov, A. F.; Bloino, J.; Zheng, G.; Sonnenberg, J. L.; Hada, M.; Ehara, M.; Toyota, K.; Fukuda, R.; Hasegawa, J.; Ishida, M.; Nakajima, T.; Honda, Y.; Kitao, O.; Nakai, H.; Vreven, T.; Montgomery, J. A., Jr.; Peralta, J. E.; Ogliaro, F.; Bearpark, M.; Heyd, J. J.; Brothers, E.; Kudin, K. N.; Staroverov, V. N.; Keith, T.; Kobayashi, R.; Normand, J.; Raghavachari, K.; Rendell, A.; Burant, J. C.; Iyengar, S. S.; Tomasi, J.; Cossi, M.; Rega, N.; Millam, J. M.; Klene, M.; Knox, J. E.; Cross, J. B.; Bakken, V.; Adamo, C.; Jaramillo, J.; Gomperts, R.; Stratmann, R. E.; Yazyev, O.; Austin, A. J.; Cammi, R.; Pomelli, C.; Ochterski, J. W.; Martin, R. L.; Morokuma, K.; Zakrzewski, V. G.; Voth, G. A.; Salvador, P.; Dannenberg, J. J.; Dapprich, S.; Daniels, A. D.; Farkas, O.; Foresman, J. B.; Ortiz, J. V.; Cioslowski, J.; Fox, D. J. ; Gaussian, Inc.: Wallingford, CT, **2009**.

(44) Schaftenaar, G.; Noordik, J. H., Molden: A Pre- and Post-Processing Program for Molecular and Electronic Structures. *J. Comput.-Aided Mol. Des.* **2000,** *14* (2), 123-134.

(45) *The PyMOL Molecular Graphics System*, 2.0; Schrödinger: LLC, 2015.

(46) Mosmann, T., Rapid Colorimetric Assay for Cellular Growth and Survival: Application to Proliferation and Cytotoxicity Assays. *J. Immunol. Methods* **1983,** *65* (1-2), 55-63.

Table of Contents Graphic

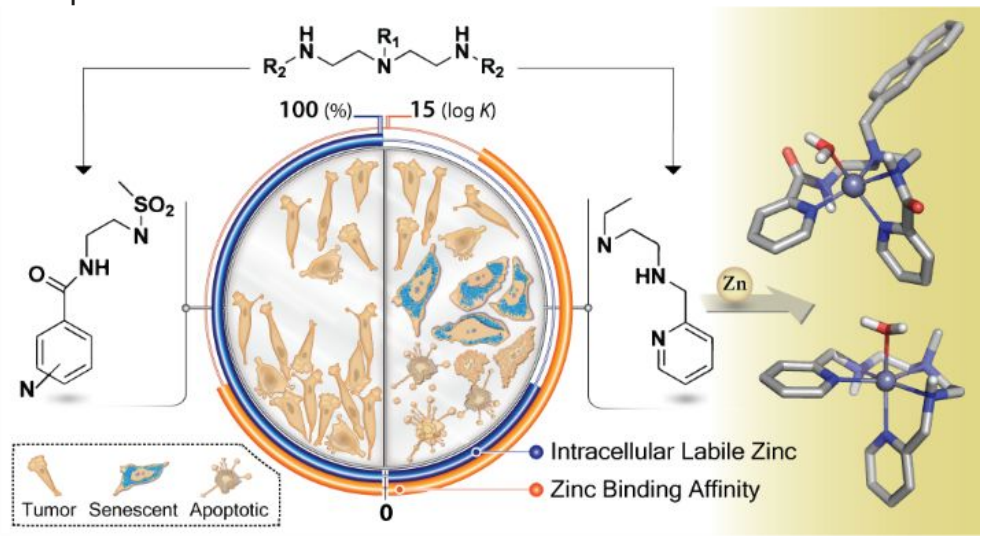

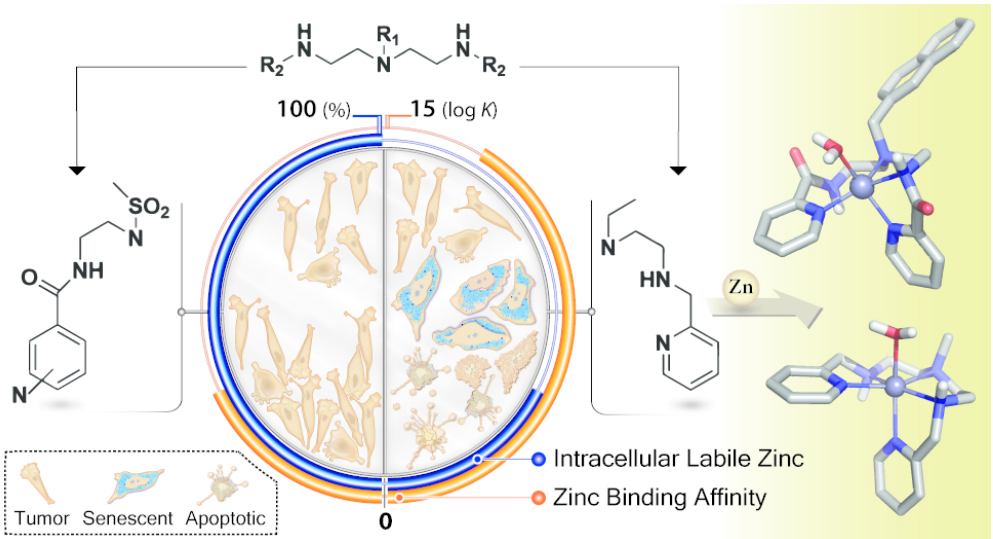

Table of Contents Graphic